LAWRENCE
LIVERMORE
NATIONAL
LABORATORY

LLNL-TR-674938

Final Report for NA-22/DTRA Cosmic Ray Project

R. E. Wurtz, G. F. Chapline, A. M. Glenn, L. F. Nakae, I. A. Pawelczak, S. A. Sheets

July 21, 2015

Disclaimer

This work performed under the auspices of the U.S. Department of Energy by Lawrence Livermore National Laboratory under Contract DE-AC52-07NA27344.

Final Report for NA-22/DTRA Cosmic Ray Project

Ron Wurtz (PI)

George Chapline, Andrew Glenn, Les Nakae, Iwona Pawelczak, Steven Sheets

Lawrence Livermore National Laboratory

Summary

The primary objective of this project was to better understand the time-correlations between the muons and neutrons produced as a result of high energy primary cosmic ray particles hitting the atmosphere, and investigate whether these time correlations might be useful in connection with the detection of special nuclear materials. During the course of this project we did observe weak correlations between secondary cosmic ray muons and cosmic ray induced fast neutrons. We also observed strong correlations between tertiary neutrons produced in a Pb pile by secondary cosmic rays and minimum ionizing particles produced in association with the tertiary neutrons.

Prior Work

For many years now, our group has been developing the theory of fission chains, and comparing theoretical predictions with experiment and Monte Carlo simulations. We have found that the interplay between simulations and experiments is essential to understanding the time-correlated particles signatures of multiplying assemblies. One problem that has persistently hampered our understanding of time correlated signals though is a proper understanding of particle correlations in the cosmic ray background.

One of our first experiments aimed at understanding the correlated signals in cosmic ray bursts was carried out in 2006, and involved using He3 neutron detectors and plastic muon detectors to study the interaction of cosmic rays bursts with a 1 ton Pb pile. One unanticipated result of this experiment, illustrated in Figure 1, was the occurrence of very large bursts of neutrons several times a day.

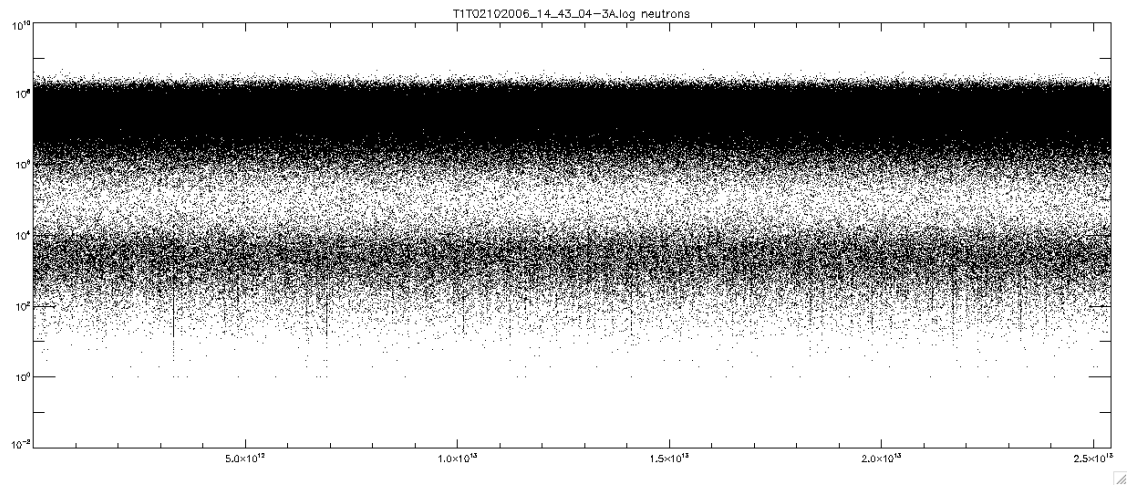

Fig 1 Time interval between successive cosmic neutrons in the presence of a Pb pile

The horizontal axis is elapsed time in shakes (10^{-8} sec), while the vertical axis shows the logarithm of the time interval between 2 successive neutrons. The figure shows 3 days of data on the time interval between successive neutron counts in the He3 detectors. The dark band at the top has time intervals typically greater than a second, and is mostly due to the neutron background. The lower band, from about 1/10 microsecond to 100 microseconds, is from correlated events. The large showers show as long streaks. One of the most intriguing results of these measurements, shown in Figure 2 , was that very large neutron bursts seemed to be always accompanied by muons, whereas smaller bursts of neutrons were not always accompanied by a muon.

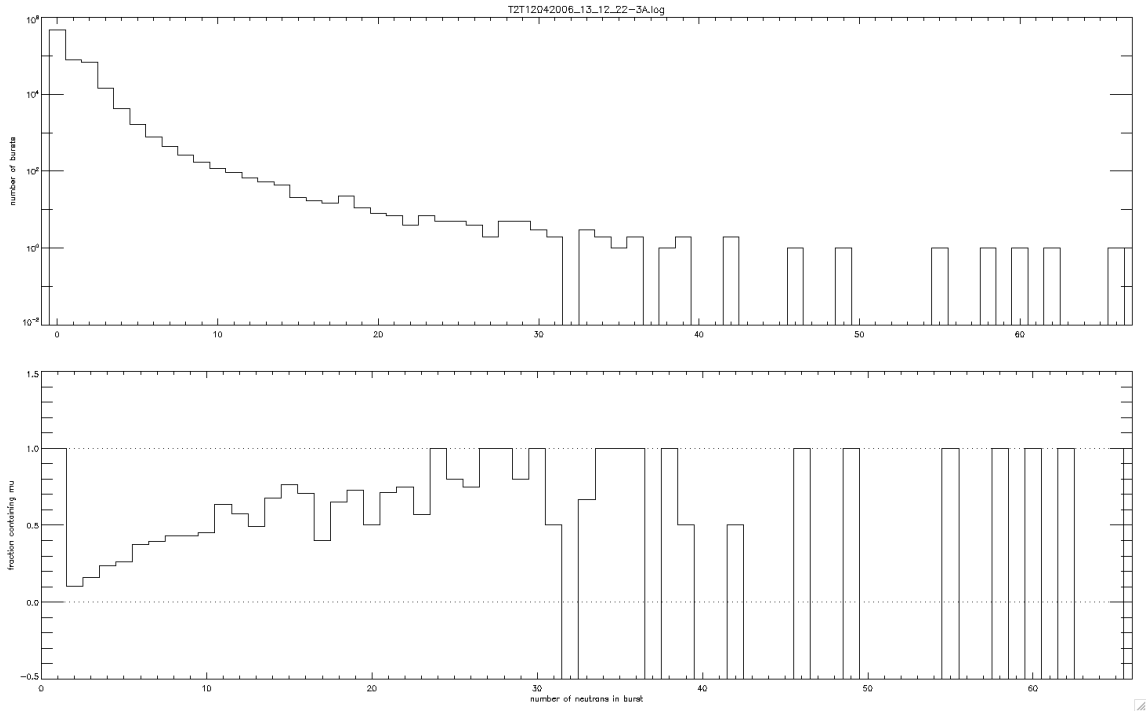

Fig 2 Results of 2006 experiment. Upper graph: number of fast neutron bursts on a logarithmic scale vs the observed size of the burst. Lower graph: fraction of bursts containing at least one minimum ionizing particle signal in the plastic "muon" panels.

The exact nature of the cosmic ray bursts giving rise to the large neutron bursts, and the frequency of these events has, up to the present time, been unclear. In addition, the high degree of correlation between what appeared to be cosmic ray muons with large neutron bursts was puzzling. One of our main objectives in this project has been to try and understand whether or not the minimum ionizing particles (MIPs) that accompanied the large neutron bursts observed in this experiment were indeed cosmic ray muons or minimum ionizing particles produced in the Pb pile.

Following our 2006 Pb pile experiment the production of neutrons by a Pb pile were also investigated by a group at Pacific Northwest National Lab [R. Kouzes, et. al. Nuclear Instruments and Methods, A587, 89 (2008)].

Simulation of Cosmic Ray Showers in the Atmosphere

In parallel with our experimental effort we have carried out simulations of the atmospheric showers induced by primary protons with various energies and their effect on our experimental apparatus using the LANL Monte Carlo code MCNP. Figure 3 shows the well known spectrum of primary cosmic ray protons that we used as input for the MCNP simulations. The atmosphere was modeled as a stack of 30 layers of air, each approximately 1 km thick, with an integrated column density of 1000 gm/cm^2 corresponding to an altitude close to sea level. The densities of the layers were derived from a standard density profile model for the atmosphere at mid-latitudes.

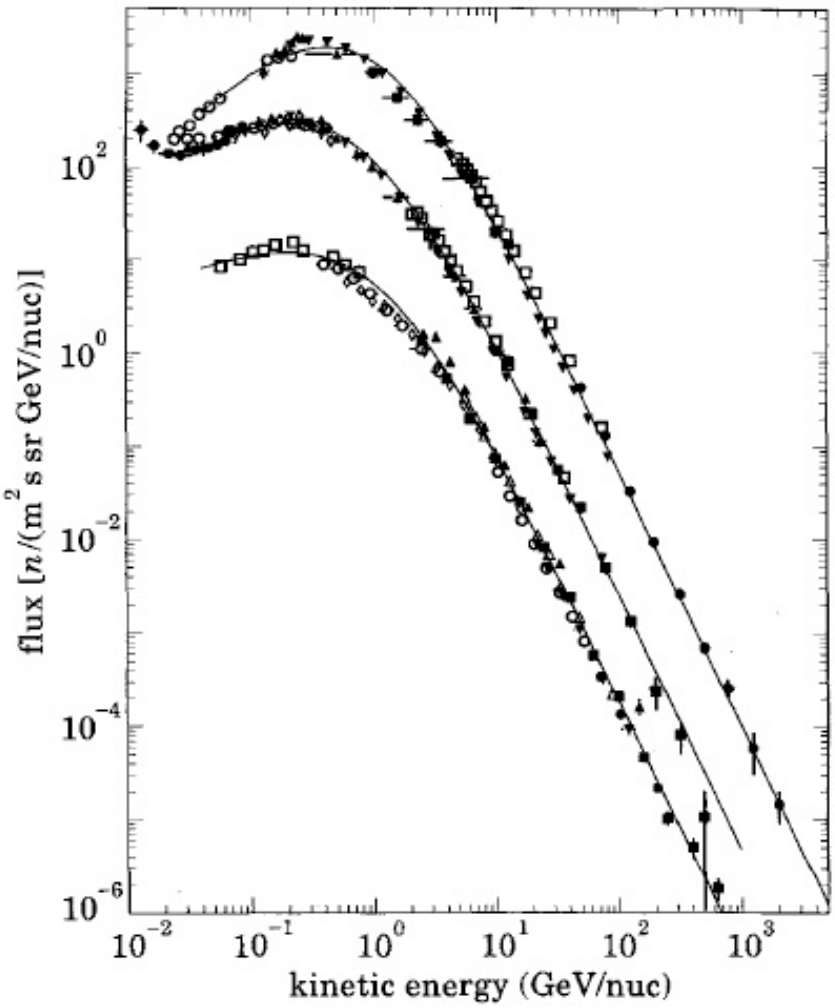

Fig 3 The measured spectrum of protons, He nuclei, and carbon nuclei in primary cosmic rays which we used as input for our simulations (taken from Papini et. al. Rev. Mod. Phys. 68, 611, 1996).

Figure 4 shows the cumulative results of MCNP simulations of 100 atmospheric showers produced by 1, 10, and 100 TeV primary protons incident on the top of the atmosphere. It should be noted that the atmospheric showers initiated by primary protons with energies near to the maximum of the primary spectrum do not typically reach the ground. Indeed secondary particles typically reach the ground only for showers initiated by primary protons with energies greater than about 10 GeV. The number of muons and neutrons with energies greater than 1 MeV (which is the energy threshold of our detectors for neutron detection) hitting the ground for various primary proton energies and incident angles (cosmic ray muons have an approximately $\cos^2\theta$ angular distribution) are shown in Fig 5.

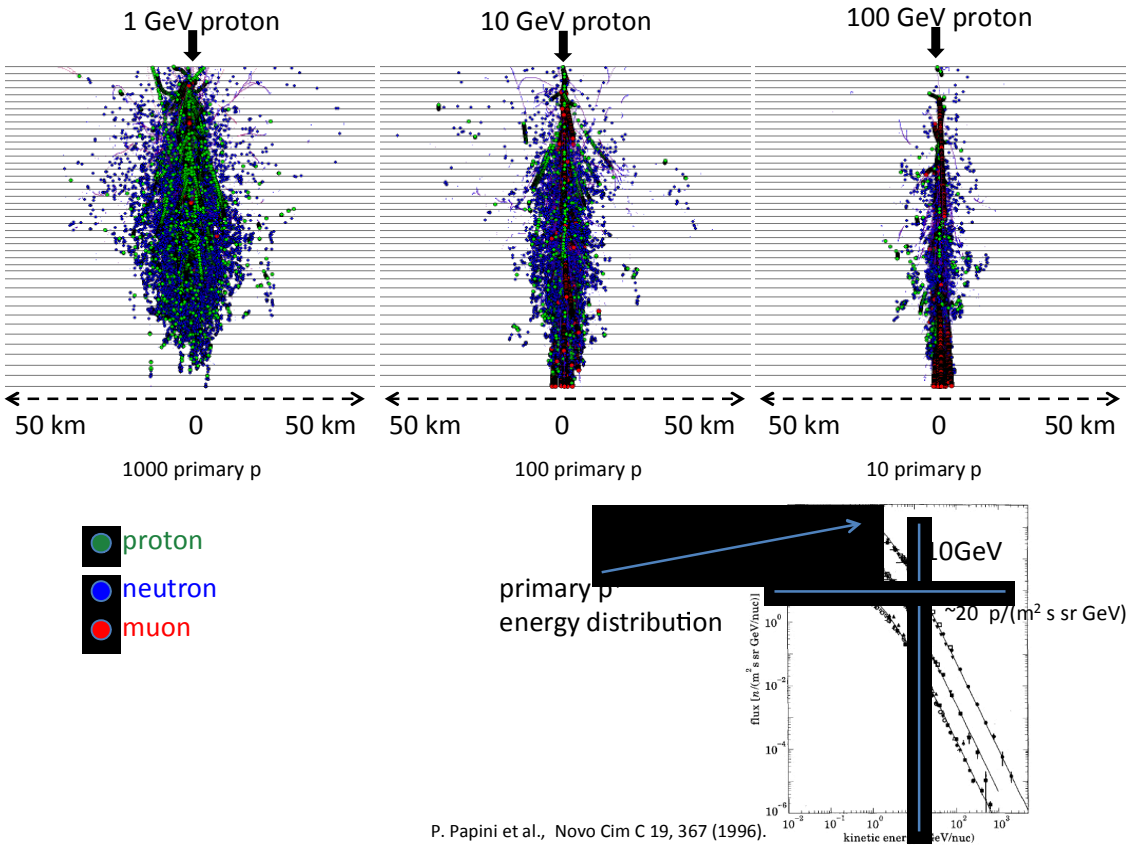

Fig 4. Monte Carlo simulations of 100 atmospheric showers produced by 1, 10, and 100 GeV primary protons incident on the top of the atmosphere. Typically only primary protons with energies greater than ~ 10 GeV produce atmospheric showers where the secondary particles reach the ground. This is the main reason why the average flux of secondary cosmic ray particles at ground level is much smaller than the average flux of primary protons at the top of the atmosphere.

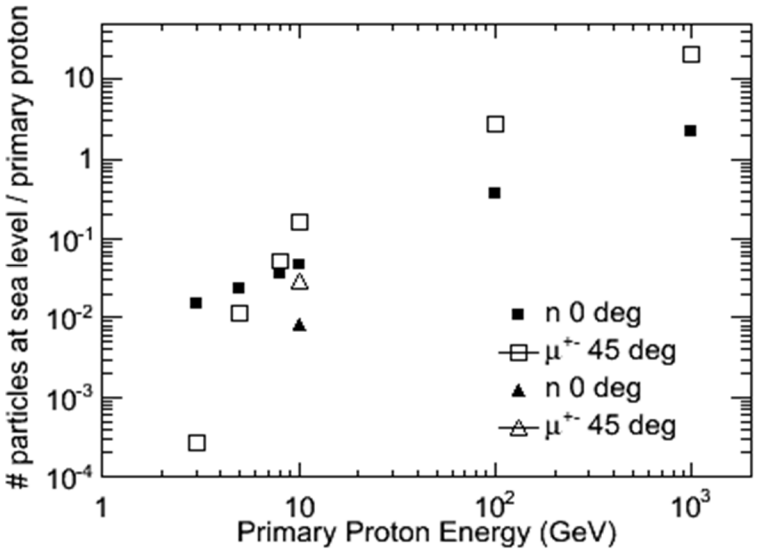

Fig 5. Number of neutrons and muons per shower as a function of primary energy

Evidently in order to get on average at least one secondary cosmic ray muon or neutron hitting the ground as a result of a single shower one needs a primary proton energy exceeding ~ 10 Gev. In order to convert the numbers of muons and neutrons per shower shown in Figure 5 into time average ground level fluxes for muons and neutrons one must multiply by the numbers shown in Figure 5 by the flux of the primary protons at the top of the atmosphere for the primary energies of interest. The result is shown in Figure 6. It can be seen the average flux of secondary muons and neutrons at sea level is a maximum for primary protons with energies on the order of 10 GeV. In fact, the flux of secondary muons and neutrons due to primary protons with energies between 8 and 15 GeV accounts for approximately 80% of the total cosmic ray flux of these of these particles at sea level. Thus in order to understand the "typical" phenomenology of secondary cosmic rays as observed at sea level it is reasonable as a first approximation to simply restrict one's attention to primary protons with energies near to 10 GeV. Restricting the energy range of primary proton energies sampled in a Monte Carlo simulation has the computational advantage that it significantly reduces the computer time needed to obtain good statistics for the secondary cosmic ray particles hitting our detectors. This is especially important when one is interested in evaluating the time correlations between secondary cosmic ray particles.

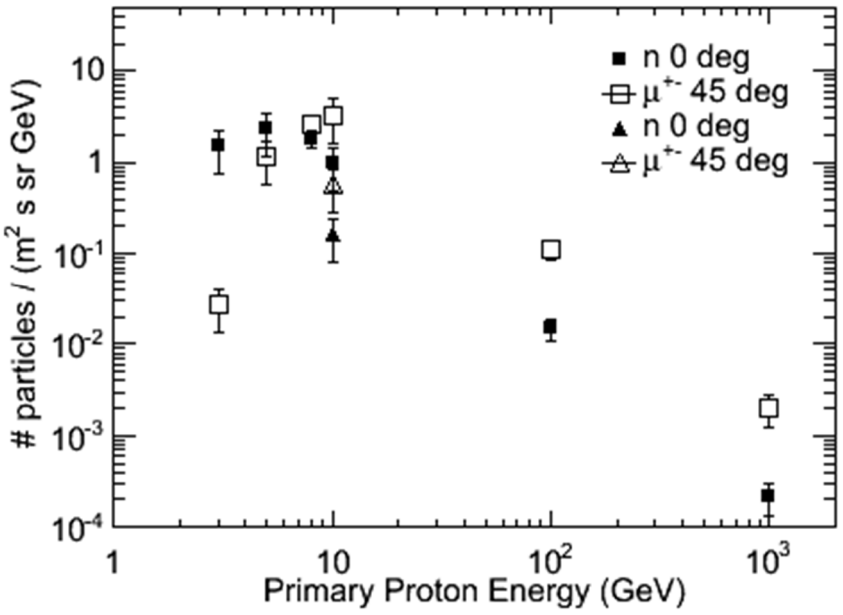

Fig 6. Average neutron and muon flux at sea level as a function of primary energy

One thing that is immediately evident from Figures 4 and 5 is that it will be very difficult to observe time correlations between secondary cosmic ray muons and neutrons with our detector array which is only ~ 3m across, since the few muons and neutrons in typical showers are typically separated by distances on the order of kilometers. In particular, the joint probability for detecting both a muon and a fast atmospheric neutron in a typical cosmic ray shower will be very small due to the fact that the average number of atmospheric neutrons produced per muon is < 1, and their spatial separation when they hit the ground will apparently be much larger than the size of our detector array (the lateral distance shown in Figure 4 is 100 km). Furthermore even when a shower does yield a muon and a fast neutron at ground level, their arrival times are typically quite different (~ 100s of μsecs),

However, our Monte Carlo simulations have shown that there are significant time correlations between secondary muons and neutrons associated with atypical events where a primary cosmic ray proton or nucleus penetrates to the lower atmosphere before interacting. Some Monte Carlo simulations of events of this type are shown in Figure 7, where it is assumed that the primary proton penetrates to an altitude of 2 km before interacting. The rate of these events is reduced by a relative to the rate of typical cosmic ray showers due to attenuation of the flux of primary cosmic ray particles by the atmosphere. Nevertheless cosmic ray showers initiated by primary protons penetrating to the lower atmosphere may be a prolific source of muon-neutron correlations. For one thing whereas typical cosmic ray showers typically contain less than 1 neutron per primary proton at ground level, the primary protons which penetrate to the lower atmosphere before interacting, will

typically contain a few neutrons. In addition, the lateral extent of Figure 7 is 15 km, so the density of muons and neutrons reaching the ground for this type of event is much higher than for the typical showers shown in Fig 4. Furthermore the rate for these types of events is not as small as one might naively estimate from the attenuation of the primary flux in the atmosphere. For example, whereas the flux of primary protons penetrating to 2 km is only 0.1% of the primary flux at the top of the atmosphere, the effective rate for these interesting events at ground level is ~ 10% the total rate of cosmic ray showers at ground level.

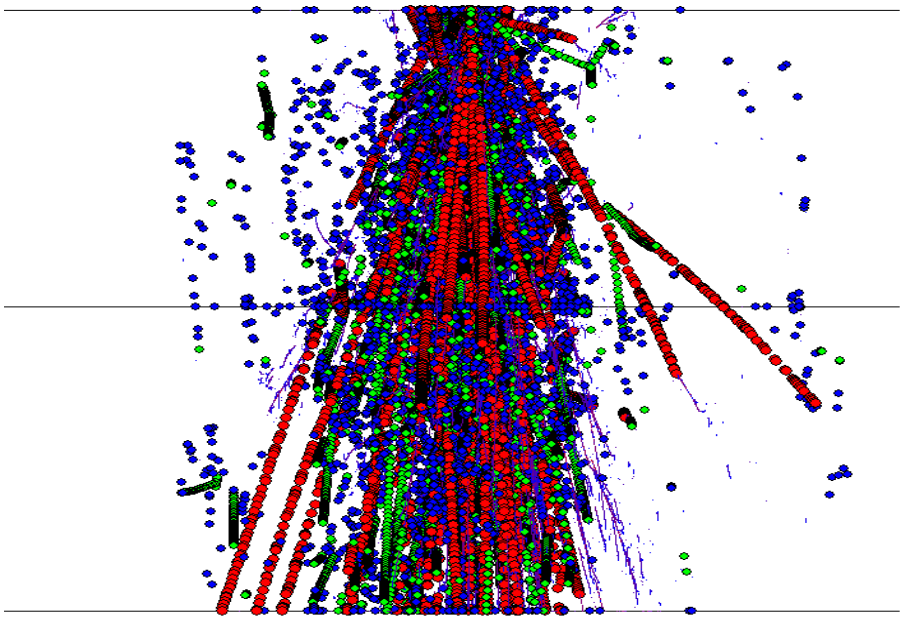

Fig 7 Monte Carlo simulations of 100 atmospheric showers produced by a 5 GeV proton incident on 2 km of air. The lateral extent of the figure is 15 km.

In Figures 8 and 9 we show the separations on the ground between muons and secondary neutrons for 10^6 showers initiated by 5 GeV primary protons interacting at a 1 km altitude and 10 GeV protons incident on 2 km of air. In contrast with the results for typical cosmic ray showers, it is now highly likely that both a muon and secondary high energy neutron or proton from the same shower will cross our array. Furthermore the average separation between the muon and neutron in these showers is much smaller that for typical cosmic ray showers (cf. Fig 4). If we assume that our 3m diameter detector array has a 10% intrinsic efficiency for detecting high energy neutrons, our simulations suggest that the count rate for this type of muon-neutron coincidence may be ~ 1 per hour. Although the numbers of muons and neutrons per primary proton is greater for a 10 GeV primary proton (1 muon and 1.9 neutrons per primary proton) than for a 5 GeV primary proton 0.6 muons and 1.8 neutrons per primary proton), the muon-neutron correlation is weaker for the 10 GeV primary protons, particularly at small separations.

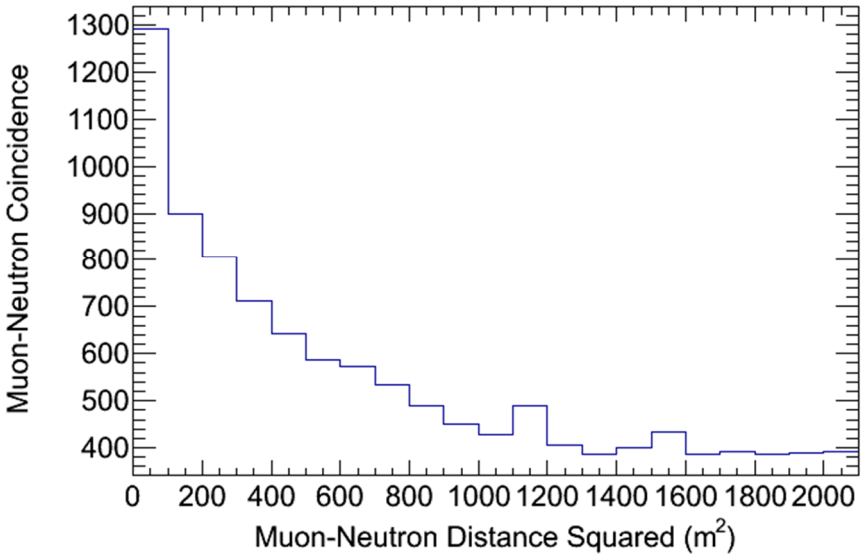

Fig 8 Radial distribution of high energy neutrons hitting the ground following a muon for 5 GeV protons incident on 1 km of air.

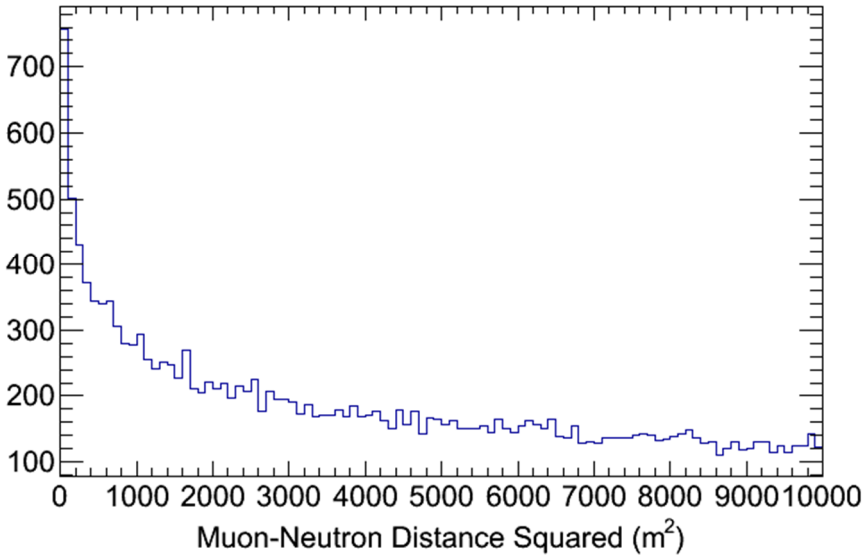

Fig 9 Radial distribution of fast neutrons hitting the ground following a muon for 10 GeV protons incident on 2 km of air.

Figures 10 and 11 show our simulations for the distributions of time delays between a muon hitting the ground and a fast neutron hitting the ground for showers initiated by 5 GeV primary protons interacting at 1 km and 10 GeV protons incident on 2 km. The average time delays are similar to the time delay for neutrons produced in the soil by μ-capture, although the slow fall-off of the distribution with

time delay is quite different from the exponential fall-off expected for muon capture neutrons.

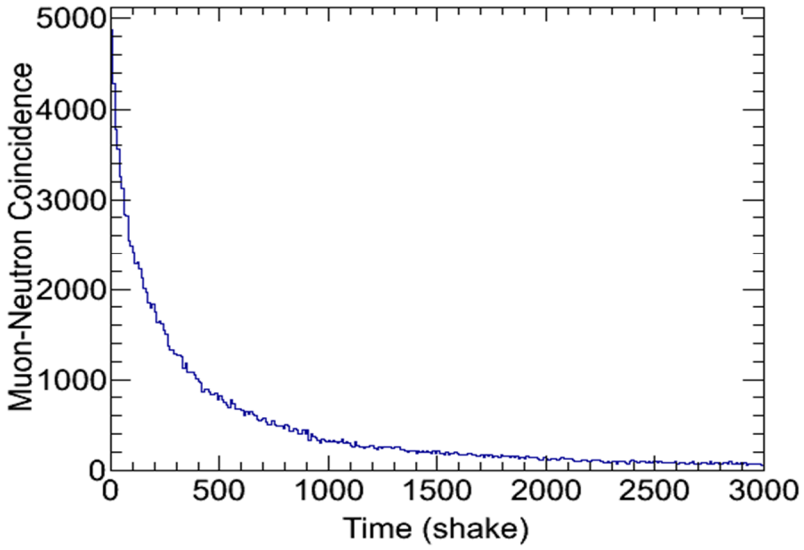

Fig 10 Monte Carlo prediction for the time delay distribution between a muon hitting the ground and a fast neutron hitting the ground for 5 GeV protons incident on 1 km of air

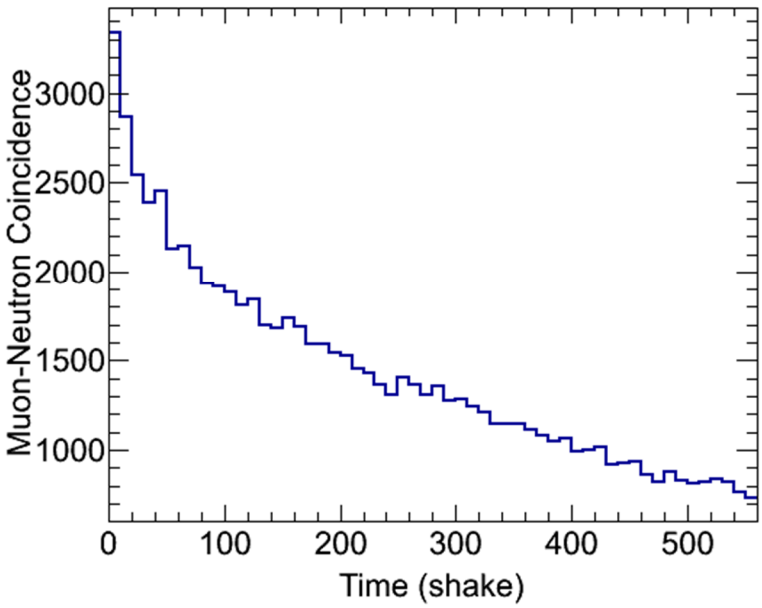

Fig 11 Monte Carlo prediction for the time delay between a muon hitting the ground and a fast neutron hitting the ground for 10 GeV protons incident on 2 km of air

In Figure 12 we show our Monte Carlo prediction for the ground level spectrum of secondary neutrons, protons, and muons due to primary cosmic ray protons with energies exceed 10 GeV. In Figure 13 we show the same spectra if the energy of the primary proton is 1 TeV. In the case of typical showers the energy of the secondary neutrons and protons is almost always below 10 GeV. Therefore in order to explain very large neutron bursts one needs primary energies much higher than the primary proton energies responsible for typical showers. We believe that showers produced by primary protons with energies greater than about 1 TeV provide a good model for the source of the high energy secondary neutrons and protons responsible for the largest neutron bursts seen in our 2006 and current experiments. As is evident from Figure 13 the numbers of secondary neutrons, protons, and muons in TeV showers is an order of magnitude higher than the average for all showers.

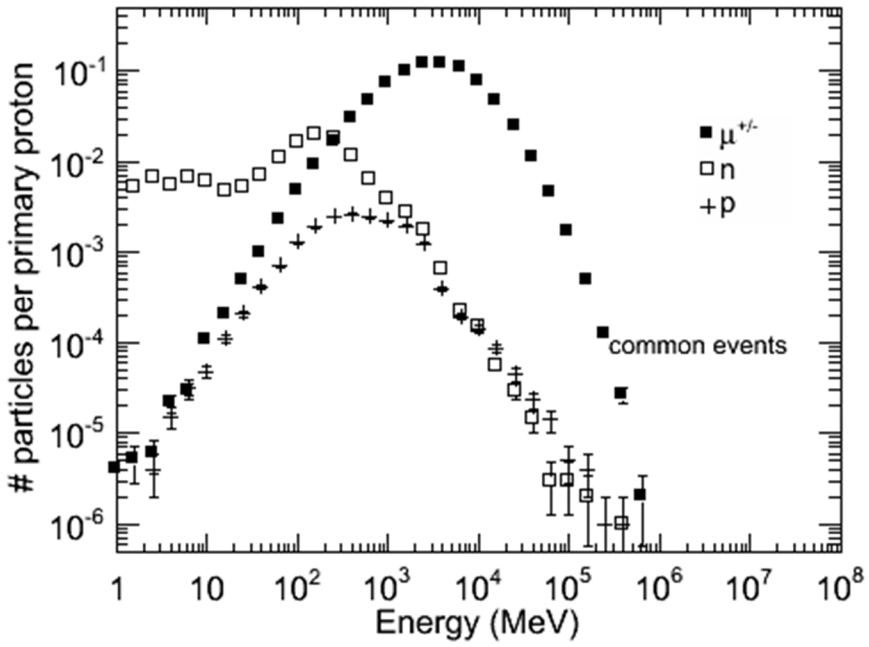

Fig 12. Monte Carlo prediction for the sea level spectrum of secondary neutrons, protons, and muons produced by primary protons with energies greater than 10 GeV.

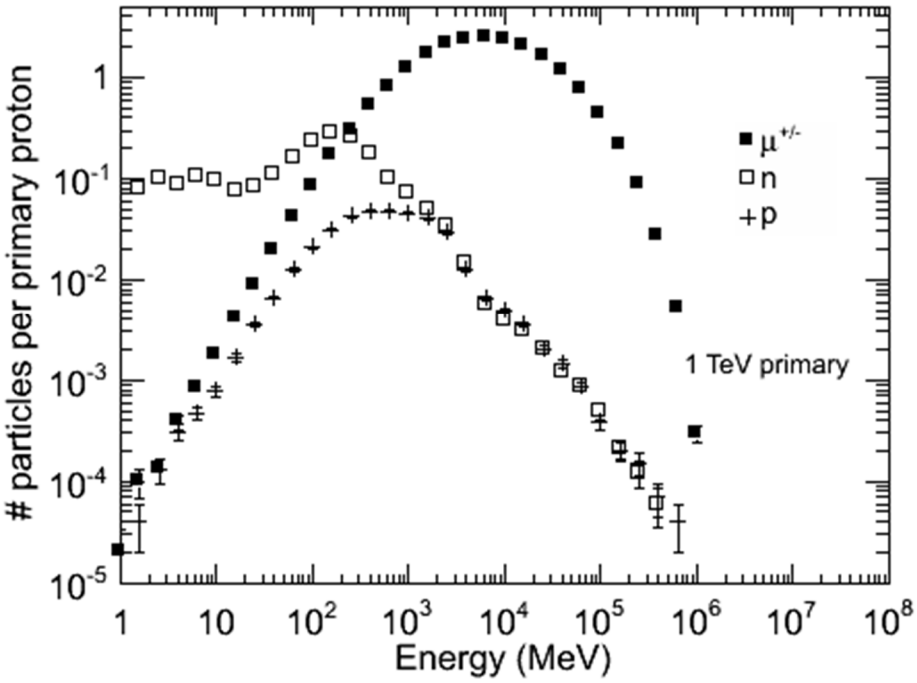

Fig. 13. Monte Carlo prediction for the ground level spectrum of secondary neutrons, protons, and muons produced by a 1 TeV primary proton normally incident on the top of the atmosphere.

Simulation of Muon–Neutron Correlations Due to Muon Capture

Apart from the correlations between secondary cosmic ray muons and neutrons, our simulation results have revealed another potentially interesting source of muon-neutron correlations. The simulations of secondary particles shown in Fig 4 did not take into account the effect of the ground. The ground can affect muon-neutron correlations in 2 ways: 1) the secondary neutrons in cosmic ray showers will be reflected off the ground, and 2) the cosmic ray muons will lose kinetic energy when the enter the ground due to ionization; after the muons come to rest they will form muonic atoms and either decay or be captured by the atomic nucleus. Capture of a muon by an atomic nucleus creates a highly excited nuclear state, resulting in the emission of fast neutrons. Figure 14 shows how the flux of secondary muons from typical showers decreases as a function of depth in the soil. Although the muon flux decreases only slowly with depth, only the fast neutrons resulting from μ-capture at relatively shallow depths will be observed due to neutron moderation and capture. Figure 15 shows the number of fast neutrons per muon reaching the surface as a function of depth. Averaging over all depths our simulations show that total number of fast neutrons per muon reaching the surface is approximately .005.

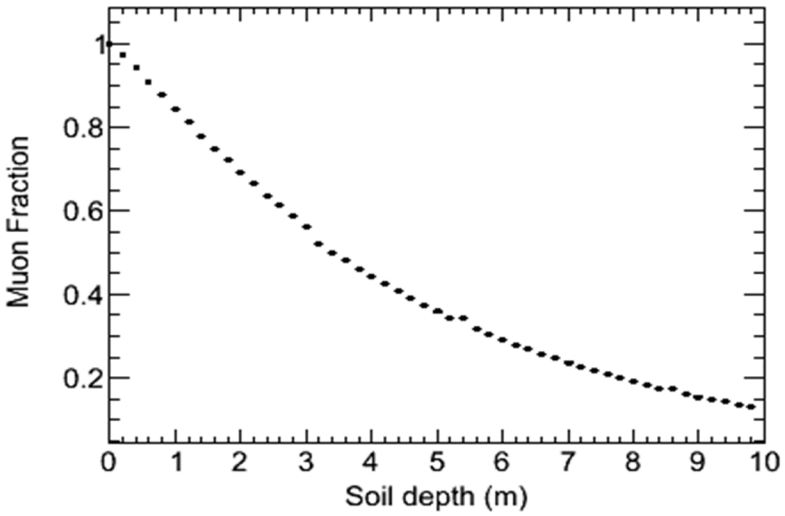

Fig 14. Fraction of cosmic ray muons remaining as a function of soil depth.

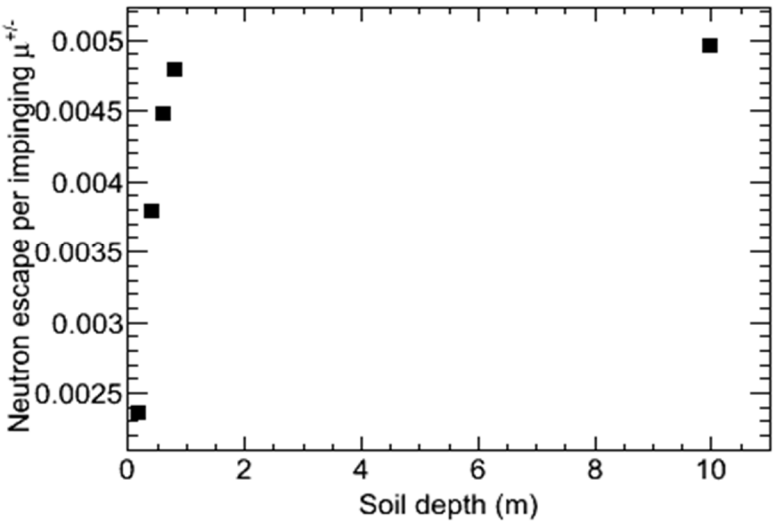

Fig 15. Fraction of μ-capture **neutrons escaping to the surface of "typical" soil as a function of the depth where the muon stops.**

The mean lifetimes of the muonic atoms for the elements with the highest abundance in "typical" soil (Eckhause Nucl. Phys 81, 575, (1966)) are: 1) Oxygen 1812 ns, 2) Si 767 ns, 3) Ca 343 ns, 4) Fe 206 ns. The fraction of μ-captures producing at least 1 fast neutron varies from about 50% for low Z atoms to nearly 100% for high Z atoms. Taking into account the transit times for the muon to come to rest and the μ-capture neutrons to reach the surface of the soil, we expect that after a secondary cosmic ray muon hits the ground, a fast neutron will emerge

from the ground about a μsec later 0.5% of the time. Figure 16 shows our simulation results for the distribution of time delays for the μ-capture neutron to reappear after a secondary muon hits the soil. The spectrum of muons used in this calculation was that for muons produced by 15 GeV primary protons hitting the top of the atmosphere and averaged over the angle of incidence. It can be seen that the slope of the time delay curve is about 1/ μsec, which is in accord with our simple estimate of the average time it takes for a muon to stop, be captured by a nucleus in the soil, and then for the neutron produced by μ-capture to diffuse to the surface.

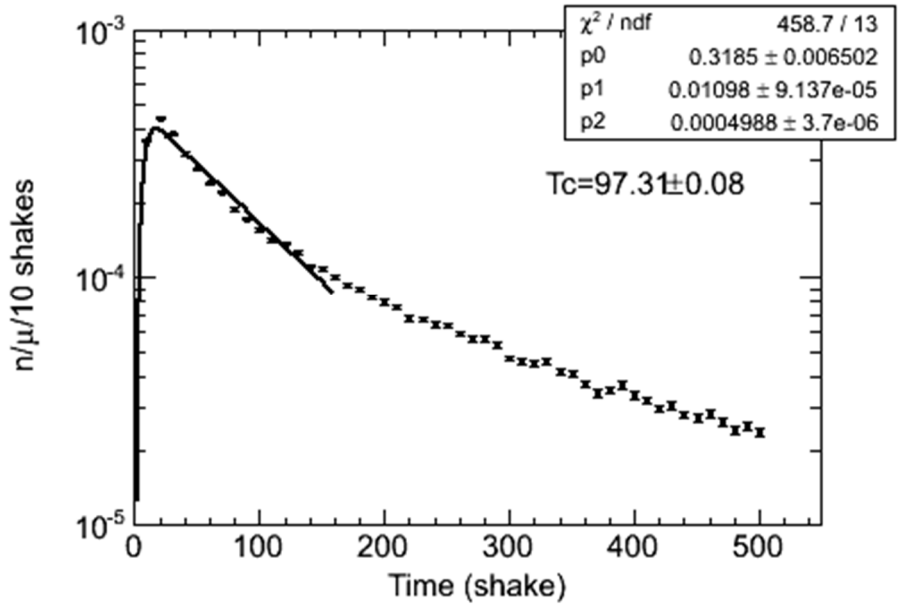

Fig 16. Time delay of μ-capture **neutrons escaping to the surface of typical soil.**

Due to the fact that neutrons produced underground can only reach the surface from a relatively shallow depth, neutrons produced by μ-capture should emerge from the ground no more than a few meters from where the muon entered the ground. Therefore our expectation is that these neutrons should dominate the muon-neutron correlations associated with typical cosmic ray showers. Indeed identification of these μ-capture neutrons will be a key test of our ability to detect μ-neutron correlations with our liquid scintillator/plastic scintillator detector array. The expected rate in our detector array for coincidences between muons and muon capture fast neutrons is expected to be on the order of 0.1 per second. Although this is much smaller than the random fast neutron background rate in our detector array (~ 10 per second), in a plot of the time delay between a muon and a fast neutron the μ-capture neutrons should show up as a prominent peak when the delay time is on the order of a μsec.

Experimental Results for Muon –Neutron Correlations at Ground Level

Our array of time tagged plastic muon detectors and liquid scintillators has observed short time correlations between muons and fast neutrons! In Fig. 17 we show the number of fast neutrons that were observed in the liquid scintillators for a 15 hour run with our detector array when a 500ns observing window was opened 1.5 μsec after a muon detection. Approximately 5000 neutrons were observed in this manner during the run, whereas the number of fast neutrons that would be expected as a result of random background events was 410. Thus the observed coincidence signal was a factor ~ 10 greater than the random background signal. This observed excess of correlated neutrons over background amounts to ~ 5 neutrons/minute. Coincidently this observed neutron signal is close to what we had expected based on our Monte Carlo simulations of fast neutron production in typical

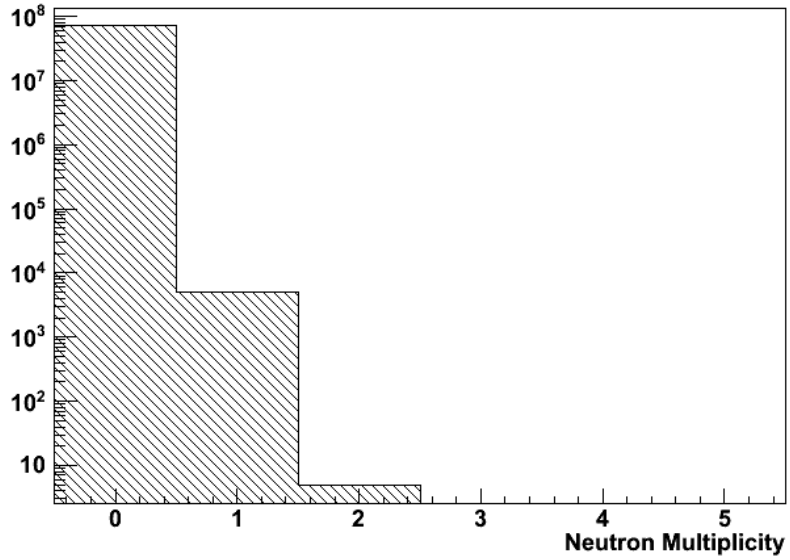

Fig 17 Observed numbers of fast neutrons counted during a 500ns interval following a detected muon with a 1.5 μsec delay during a 15 hour run.

soil due to muon capture. These initial Monte Carlo simulations suggested that ~ 5 x 10^{-3} fast neutrons per incident muon would emerge from the soil beneath our detectors (cf. Fig.15). The observed muon rate in our plastic muon detectors was 1330 muons/sec. Dividing by the area of the muon detectors (7.4m^2) and multiplying by .005 one would predict that 54 fast neutrons per square meter per second would be emerging from the soil beneath our detectors as a result of muon capture in the soil. Multiplying by the effective area of the liquid scintillator array (0.6 m^2) and taking into account that only ~ 40% of the muon capture neutrons have energies above ~ 1 MeV threshold for our detectors, we had expected that the count rate for muon capture neutrons should have been about 6/minute. This was close to the observed 5/minute rate of correlated neutrons, and led us to initially

believe that the correlated neutrons that we were seeing were almost entirely due to muon capture. However, when we analyzed how number of neutrons observed in a 500ns window depended on the time delay we reached a quite different conclusion. As shown in Fig. 20 the observed number of correlated neutrons falls off much slower with time delay than would be expected for muon capture (cf. Fig. 12).

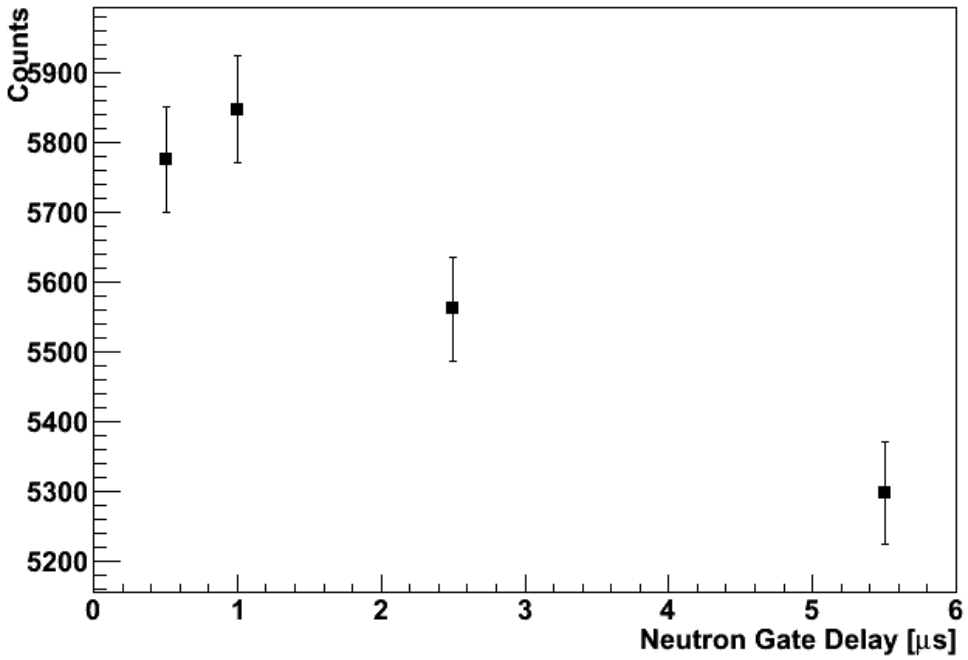

Fig 18 Observed numbers of fast neutrons counted in a 500ns window following a detected muon as a function of the time delay of the opening of the window after the muon detection.

Indeed because the muon lifetime is 2 μsec the number of correlated neutrons should fall exponentially for delay times greater than 2 μsec. Evidently the correlated neutrons that we observed were partly due to the secondary cosmic ray neutrons that accompany a muon in cosmic ray showers like the simulations illustrated in Fig.s 4 and 7. In order to understand why our initial estimate of the rate for muon capture neutrons was roughly the same as the observed rate of correlated neutrons, we reanalyzed the production of muon capture neutrons in the ground beneath our detectors, taking into account that our detector array actually sat on a layer of asphalt approximately 8 cm thick. It turned out that the presence of this hydrogen-rich asphalt layer made a very significant difference in the number of muon capture neutrons that reach the surface of the ground. The .005 survival fraction that we had previously estimated for typical soil was reduced to 8 x 10^{-4} when the 8 cm asphalt layer was taken into account, so our new estimate for the count rate due to muon capture neutrons is ~ 1/min.

Simulations of Secondary Cosmic Ray Interactions With a Pb Pile

One of our objectives in this project was to attempt to understand the origin of the large neutron bursts that were seen in our 2006 Pb pile experiment using ^{3}He neutron detectors. Neutrons are continuously produced in a Pb pile by the muons, neutrons, and protons present in secondary cosmic rays. When each of these types of particles interact with a Pb pile, tertiary neutrons and protons will be produced. In Figure 19 we show the arrangement of the cart holding a 50cmx50cmx50cm Pb pile, the packs of liquid scintillator cells, and plastic scintillator panels used in our experiment. The 1m x 1/3m x 4" plastic muon panels were placed flat on the ground surrounding the cart with the Pb pile, while the packs of 6" diameter x 6" liquid scintillator containers were stacked around the sides of the Pb pile.

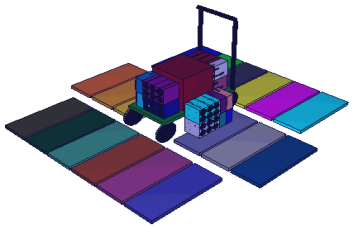

Fig. 19 Schematic diagram of detector array showing the Pb pile, liquid scintillators, and plastic muon panels.

As discussed earlier secondary cosmic rays arrive at sea level in bursts due to individual primary protons and nuclei with various energies interacting with the atmosphere, typically altitudes on the order of 15 km. In this and the following section we will be concerned with the interaction with our 50cmx50cmx50cm Pb pile of the secondary cosmic ray particles produced as a result of the interaction of the primary cosmic ray particles with the atmosphere. Since the secondary cosmic ray neutrons and protons hitting the Pb pile have a spectrum extending up to very high energies, we expect that the interactions of secondary cosmic ray particles with the Pb pile will be a source of large neutron bursts. In Figure 20 we show simulations of the size distribution for fast neutron (> 1 MeV) bursts produced by each of the main type of secondary cosmic ray particle. It can be seen that we expect that bursts containing hundreds of neutrons will be produced every day. This is in accord with what was observed in our 2006 Pb pile experiment where the neutrons were recorded with ^{3}He detectors.

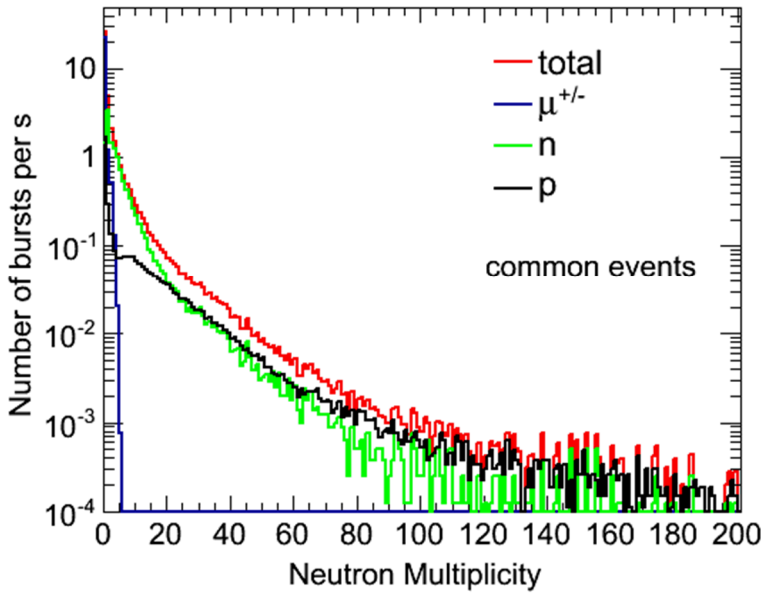

Fig. 20. **Monte Carlo prediction for the multiplicity distribution of fast neutron bursts produced in our Pb pile by secondary neutrons, protons, and muons resulting from primary protons with energies exceeding 10 GeV.**

Although secondary neutrons are responsible for most of the tertiary neutrons produced in the Pb pile, it is interesting that our Monte Carlo simulation predicts that "secondary" protons are responsible for more multiple neutron bursts than secondary neutrons. Since the spallation neutrons and protons resulting from the interactions of high energy primary and secondary particles with the atmosphere are produced in approximately equal numbers, the increased importance of secondary protons in the production of multiple neutron bursts may be due to primary protons that have either penetrated to sea level with no interaction or have only experienced forward elastic differential scattering. In order to test this hypothesis we have separately simulated the production of tertiary particles in the Pb pile due to 10 GeV primary protons that penetrated to 2 km above sea level before experiencing any interaction with the atmosphere. In Fig. 21 we show our Monte Carlo prediction for the sea level energy spectrum of the protons, neutrons and muons that appear as a result of a single 10 GeV primary proton interacting with the atmosphere at an altitude of 2 km. We interpret the peak in the proton spectrum near to 10 GeV as being due to the 10 GeV primary proton penetrating to sea level with either no interaction or only forward diffraction scattering.

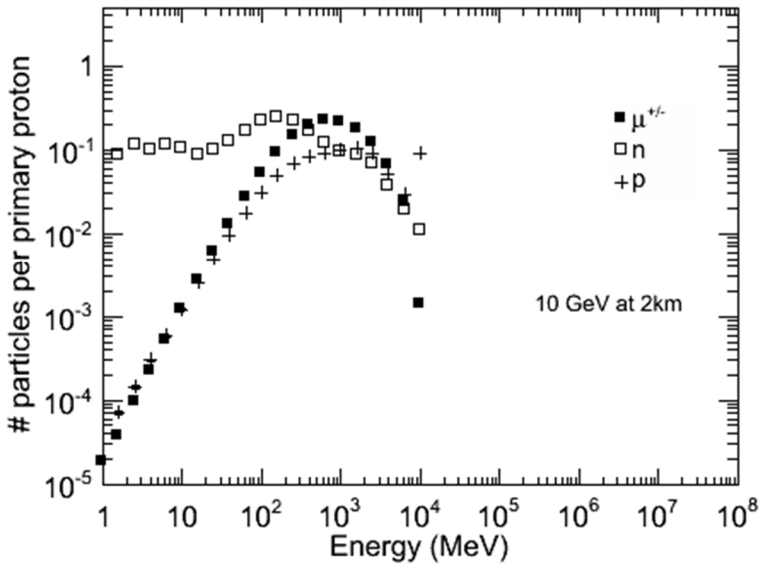

Fig 21. Monte Carlo simulation of the energy spectra for the secondary neutrons, protons, and muons resulting from a 10 GeV primary proton interacting with the atmosphere at an altitude of 2 km.

We show in Fig. 22 our prediction for the distribution of neutron multiplicities for fast neutron bursts produced in the Pb pile when secondary neutrons, protons, and muons with the spectra shown in Fig. 20 hit the top of the Pb pile. It can be seen that bursts containing more than a hundred neutrons will be produced every few hours. This is consistent with both what was observed in our 2006 Pb pile experiment where the neutrons were recorded with ^{3}He detectors and our current experiment that used liquid scintillators to detect the neutrons. It is clear that in this case that high multiplicity neutron bursts are produced mainly by secondary protons, which we interpret as being due to the contribution of the primary protons that have either had no interaction or only experienced forward diffraction scattering. The magnitude of the rates for larger bursts shown in Fig. 21 are consistent with the attenuation expected for 10 GeV primary protons passing through most of the atmosphere.

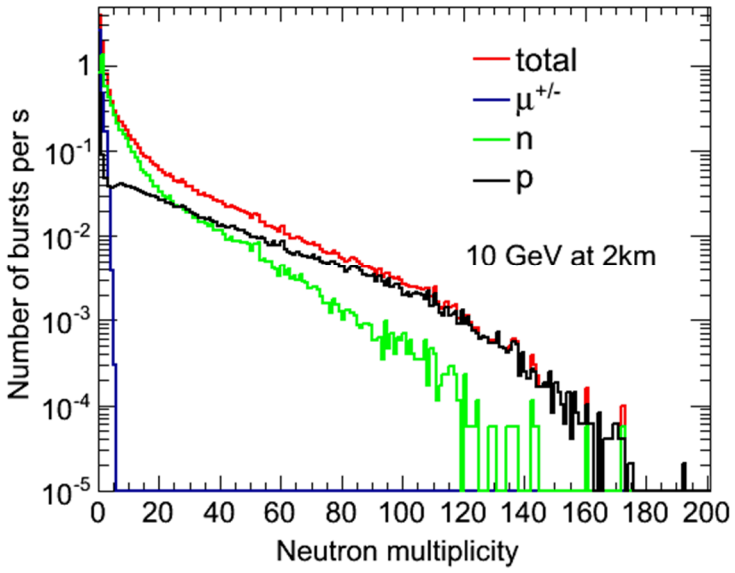

Fig. 22. Monte Carlo prediction for the rates of neutron bursts in produced our Pb pile by secondary neutrons, protons, and muons resulting from 10 GeV primary protons first interacting with the atmosphere at an altitude of 2 km.

While a 10 GeV proton interacting lower down in the atmosphere seems to be a good model for most of the neutron bursts seen in our 2006 and current experiment, we believe that secondary neutrons and protons with energies greater than 10 GeV played a crucial role in producing the largest bursts of neutrons seen in these experiments. Secondary neutrons and protons with such energies cannot be produced by by primary protons with energies on the order of 10 GeV. We show in Figure 23 the tertiary neutron multiplicities produced by TeV primary protons interacting at the top of the atmosphere. Comparing Figures 22 and 23 shows that primary protons interacting lower down in the atmosphere may dominate burst production from the Pb pile until one reaches bursts containing many hundreds of neutrons. Although these simulations were done for specific primary energies incident at different altitudes, we believe that the secondary showers produced by these relatively rare cosmic rays provide good models for the types of cosmic ray showers that are mainly responsible for the large neutron bursts produced by a Pb pile, both in our 2006 and current experiments.

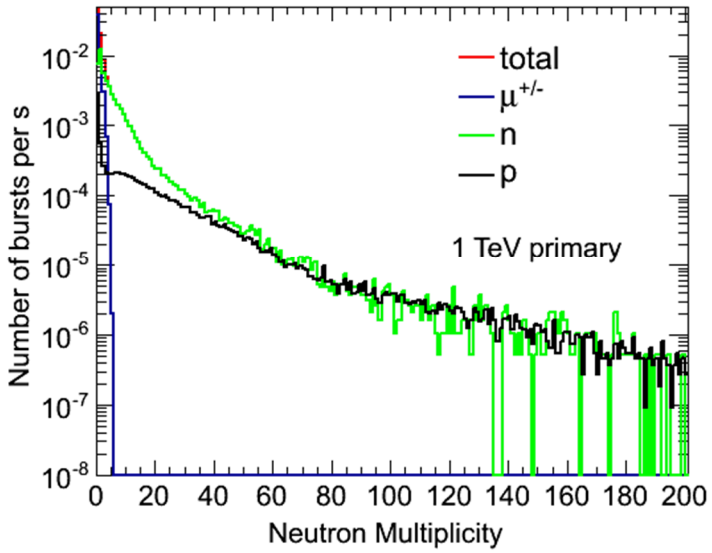

Fig. 23. Monte Carlo prediction for the rates of neutron bursts produced in our Pb pile by secondary neutrons, protons, and muons resulting from TeV primary protons hitting the top of the atmosphere.

Our Monte Carlo simulations also indicate that large bursts of fast neutrons from the Pb pile should be accompanied by comparable numbers of γ-rays with energies exceeding a few KeV. The predicted frequency of these γ-rays bursts as a function of the number of γ-rays in the burst is shown in Figure 24. It can be seen that the multiplicity distribution for these γ-ray bursts is similar to the multiplicity distribution of fast neutron bursts produced in the Pb pile. In addition to the γ-ray bursts accompanying the fast neutron bursts, the experimental results to be discussed in the following section indicate that there are also γ-ray bursts with no liquid scintillator fast neutron signal. These bursts are probably the large electromagnetic showers whose properties were the focus of a number of theoretical papers in the 1930's. Because our main focus has been on cosmic ray showers initiated by high energy protons and containing fast neutrons, we have not attempted to include electromagnetic showers in our simulations.

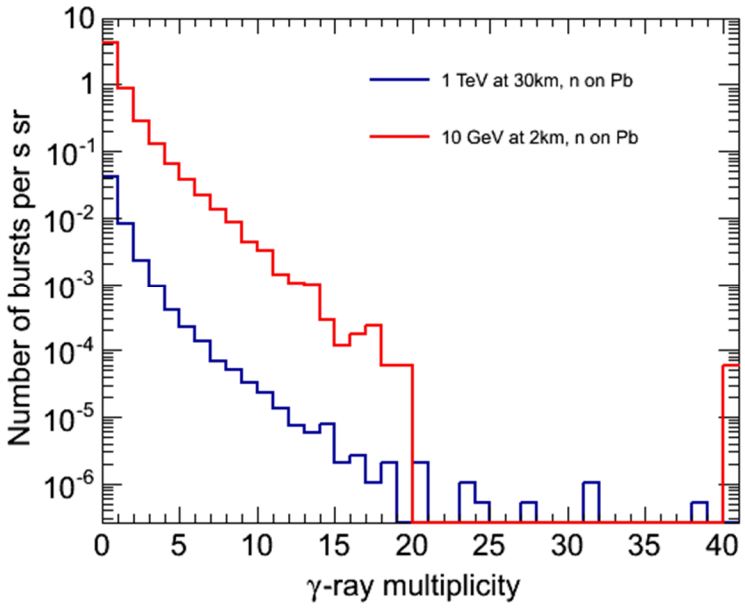

Fig. 24. Predicted multiplicity distribution for bursts of γ-rays with energies > 100 keV that would accompanying neutron bursts produced in our Pb pile.

Of course the multiplicities of fast neutron and γ-ray bursts that are actually detected will be much smaller than shown in Figures 20 and 22-24 because the overall efficiency of the liquid scintillator detectors is much less than 100%.

We now turn to the question of the MIPs that accompany the bursts of tertiary neutrons. Fortunately it is much easier to compare the Monte Carlo predictions for MIP bursts with experiment because the intrinsic detection efficiency of the plastic detectors for MIPs is nearly 100%. In Figures 25-26 we show our Monte Carlo predictions for the rate of MIP burst event multiplicities associated with the detection of at least 1 fast neutron for both "typical" cosmic ray showers and a model for the rare showers that we believe are responsible for very large bursts. These simulations suggest that primary cosmic rays with energies ~ 1 TeV are responsible for the very large bursts that we observed in our 2006 experiment.

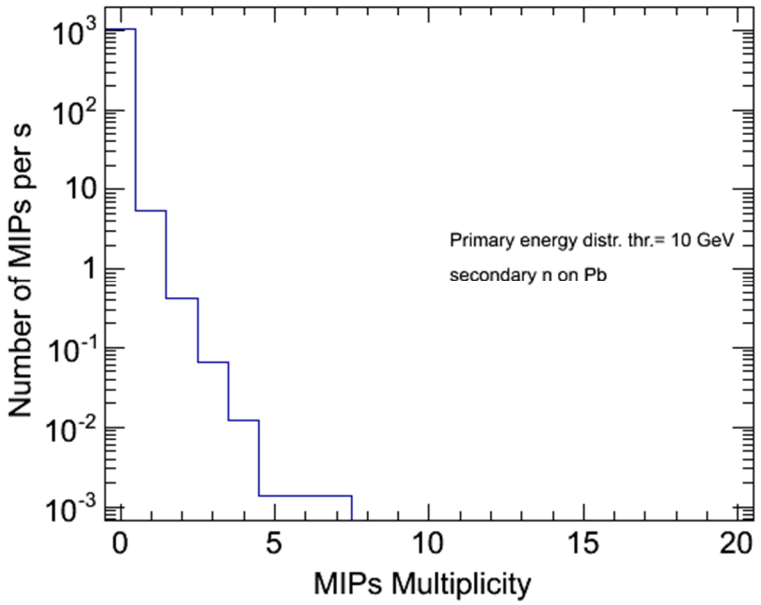

Fig. 25. Monte Carlo prediction for the multiplicity distribution of MIP particles produced in our Pb pile in association with a fast neutron by secondary cosmic ray neutrons hitting the top of the Pb pile by primary cosmic ray protons with energies > 10 GeV.

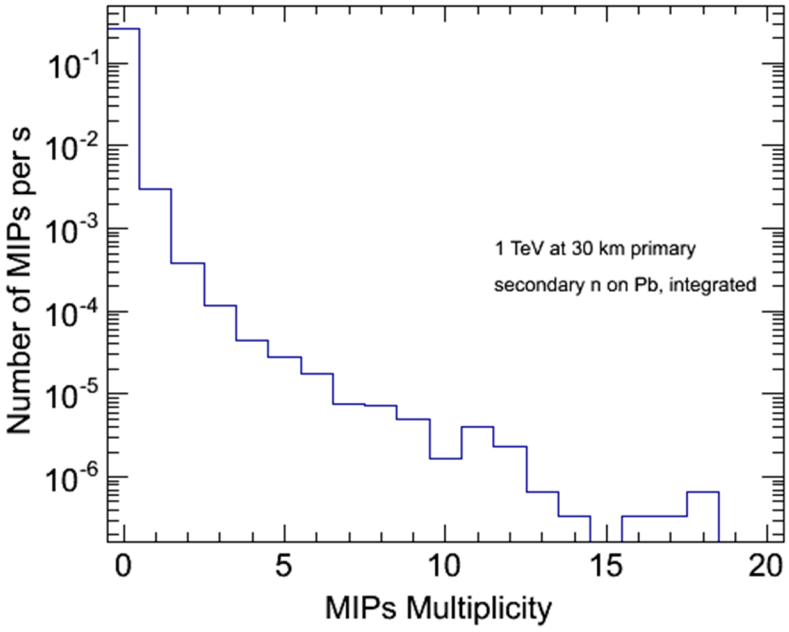

Fig. 26. Monte Carlo prediction for the multiplicity of MIP signals produced in our Pb pile in association with a fast neutron by a 1 TeV primary proton incident on the top of the atmosphere.

The geometric layout of our array of plastic detectors, together with a Monte Carlo prediction for the tertiary MIPs hitting our plastic scintillator array during a 12 minute period as a result of secondary cosmic ray neutrons hitting the top of our 50cmx50cmx50cm Pb pile is shown in Figure 27. The predicted number of MIP events falls recorded in the array falls off roughly as the inverse square of the distance of the plastic panel from the Pb pile. Also it can be seen that the sptatial distribution of the spallation protons hitting the plastic scintillator panels is asymmetric. This may be partly due to the fact that liquid scintillators on the sides of the Pb pile are located at different heights. On the top and bottom sides of Pb pile as viewed in the diagram the liquid scintillator packs were sitting on the asphalt, while on the horizontal sides as viewed in the diagram the liquid scintillator packs were sitting on the cart. The dependence of the number of protons interacting with the plastic scintillators on azimuth will reflect the difference in the probability of interacting with the liquid scintillators.

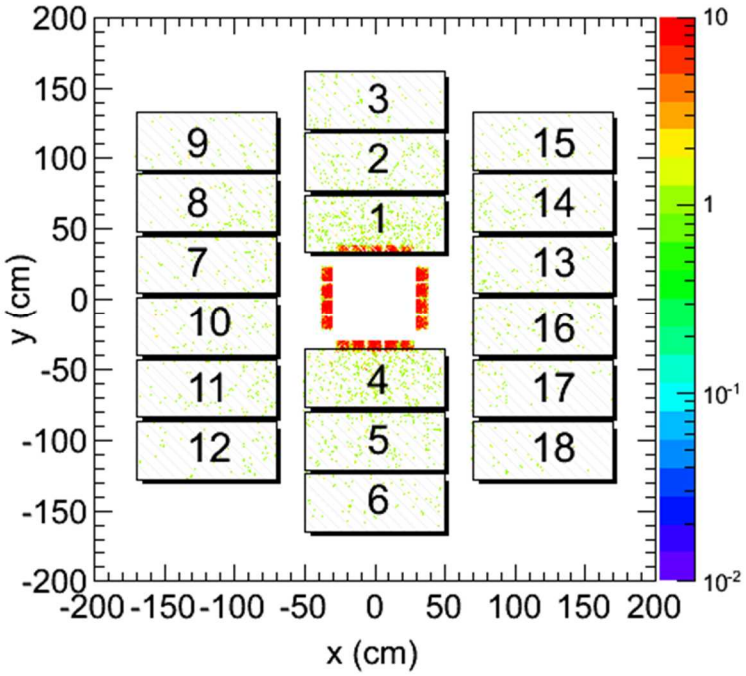

Fig. 27. Layout of the plastic scintillator array surrounding our 50cmx50cmx50cm Pb pile. The yellow crosses show a Monte Carlo simulation of the tertiary MIPs that would hit our plastic scintillator array as a result of 10^6 secondary cosmic ray neutrons hitting the top of the pile. This corresponds to an elapsed time of approximately 12 minutes.

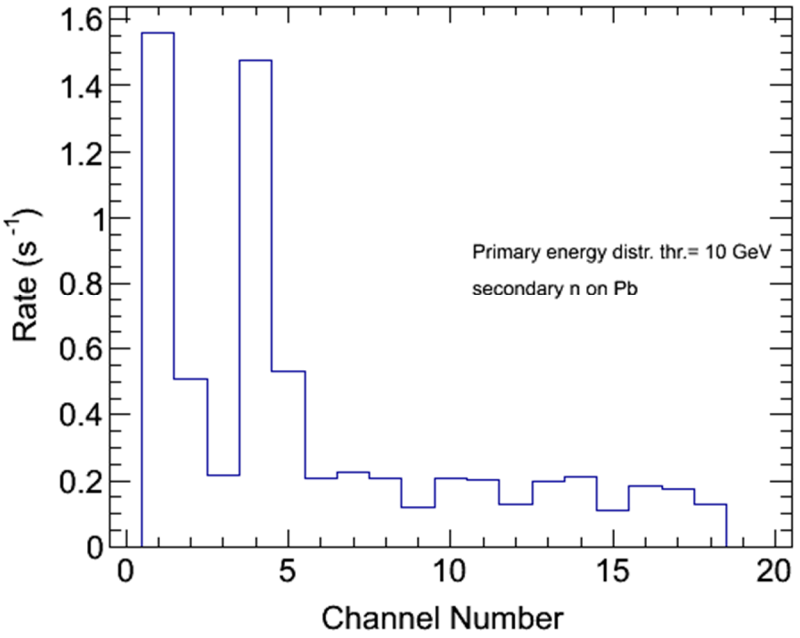

Fig. 28. Monte Carlo prediction for the spatial distribution of MIPs hitting our plastic scintillator array following a secondary neutron hitting the top of the Pb pile and a fast neutron signal in a liquid scintillator .

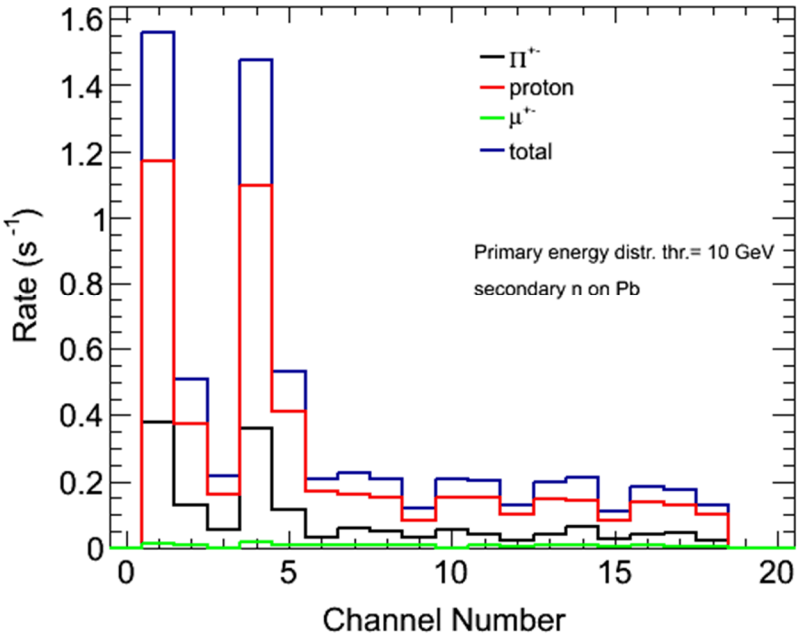

Fig. 29. Monte Carlo prediction for the separate tertiary spallation protons, pions, and muons contributions to the MIP signals shown in Fig. 28.

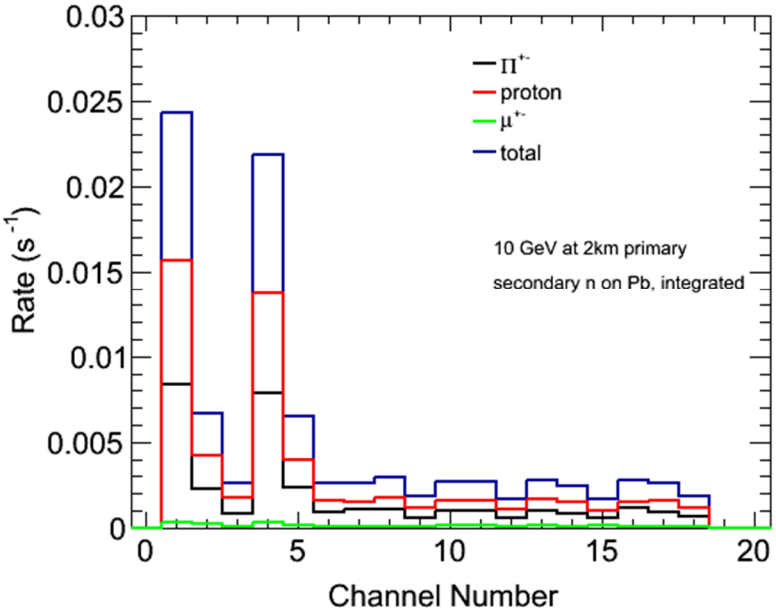

Fig. 30. Monte Carlo prediction for the composition of the MIP signals following a fast neutron liquid scintillator signal when the secondary cosmic ray neutron hitting the Pb pile results from a 10 GeV primary interacting with the atmosphere at an altitude of 2 km.

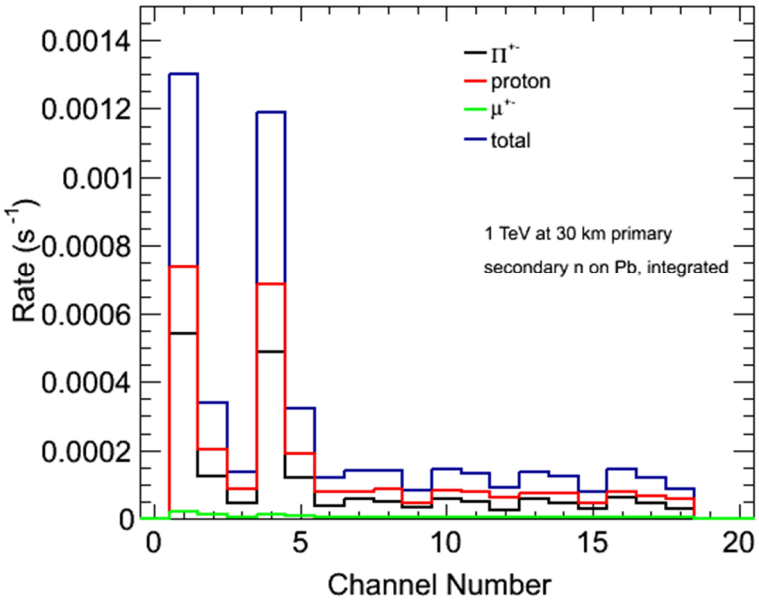

Fig. 31. Monte Carlo prediction for the composition of the MIP signals following a fast neutron liquid scintillator signal when the secondary cosmic ray neutron hitting the Pb pile results from a TeV primary proton hitting the top of the atmosphere.

A strong spatial asymmetry between the two symmetry axes of the Pb pile is evident in the data, although this is partly due to the difference in the average distance from the Pb pile of the detectors along these two axes. As is evident from Figures 29-31 the composition of the tertiary MIPs changes as a function of the size of the neutron burst from being mostly spallation protons for small bursts to mostly pions for very large bursts. In these simulations we have not attempted to construct a detailed model for the plastic scintillators, but have simply kept track of the Monte Carlo particles of various types hitting the surface of the plastic scintillators. Nevertheless we find that our approach is in reasonably good agreement with the experimental data that we will now describe.

Experimental Results for Muon –Neutron Correlations With a Pb Pile

We installed a Pb pile in the middle of our time tagged detector array as illustrated in Figure 19 in April 2013. After using a radioactive source to synchronize the timing of the signals from the various detectors, we have accumulated approximately 200 hours of data with the Pb pile and detectors in the configuration shown in Figure 21. Figure 32 shows the spectra of energy depositions in the liquid scintillator cells as recorded by the strength of the light flash recorded by the PMT in a single liquid scintillator cell. Most of these events are due to γ-rays, and the Compton edges due to the well known background Th and K γ-ray lines are clearly visible.

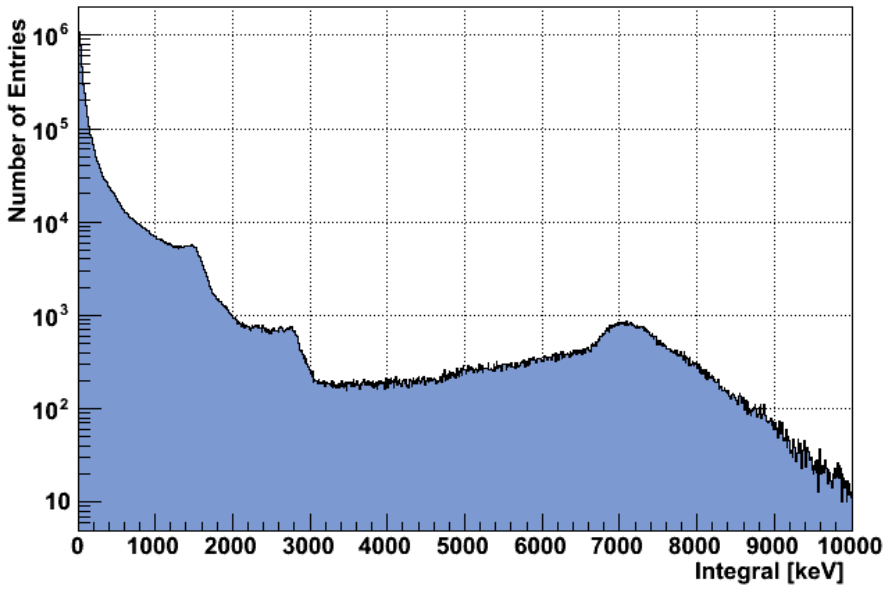

Fig. 32 Spectrum of energies deposited in liquid scintillator cells by single particle events. The peak near to 7 MeV is due to MIPs clipping the corners of the liquid scintillator cells, and depositing at least 2 MeV.

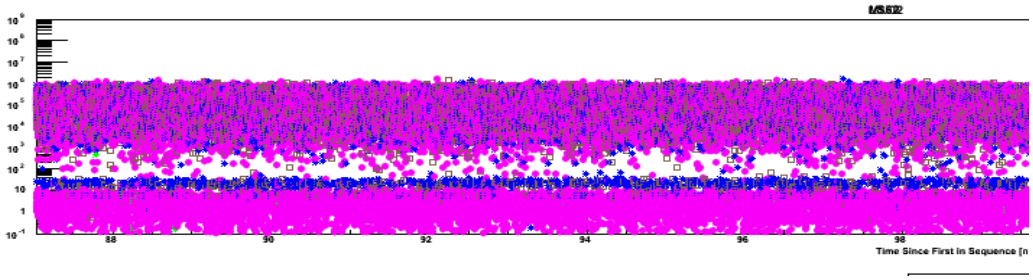

Fig. 33. “Waterfall” plot showing the time intervals between particles recorded in our liquid and plastic scintillator detectors in the presence of a 50cmx50cmx50cm Pb pile during a period of 5 days. The vertical axis is the log of the time interval between consecutive particles. Gold symbols represent fast neutrons, the blue symbols are minimum ionizing particles (MIPs), and and pink symbols are γ-rays.

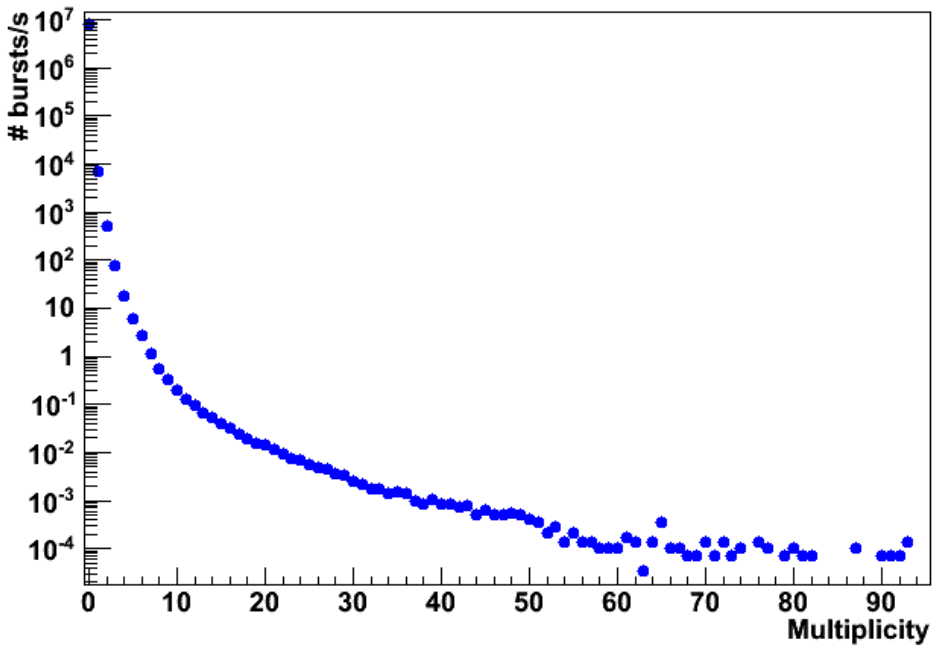

Fig. 34. Number of burst signals vs particle multiplicity recorded our array of liquid and plastic scintillators during a period of 8 hrs.

Figure 33 is a “waterfall” plot showing the time correlations between particles. The upper band of the waterfall plot is the background due to particles arriving at random times, while the lower bands show that there are many events where a particle is accompanied by other particles arriving within a short time interval which is much less than the typical spread in time it would take different secondary particles in a single shower to reach our detector array. Evidently these short

duration bursts are originating close to our array. In Figure 34 we show the multiplicity distribution for these bursts. Closer examination shows that the high multiplicity events consist mainly of γ-rays and minimum ionizing particles (MIPs). We surmise that the very high multiplicity MIPs events probably represent electromagnetic showers. Of more immediate interest for our project are showers contain fast neutrons.

In the absence of the Pb pile we had observed ~ 2 fast neutrons/sec in our liquid scintillators and, somewhat surprisingly, in the presence of the Pb pile we observed a similar count rate; i.e. the presence of the Pb pile did not noticeably increase the average fast neutron count rate. However, the number of events containing several fast neutron events increased dramatically. In Figures 34 and 35 we show the fast neutron multiplicity distribution measured by our liquid scintillator array, with and without the presence of a Pb pile. It can be seen that the presence of the Pb pile substantially increases the number of bursts with multiple neutrons. These results are consistent with the prediction of our Monte Carlo simulations that secondary cosmic rays hitting our Pb pile produce bursts containing several neutrons every minute and bursts containing hundreds of neutrons every day.

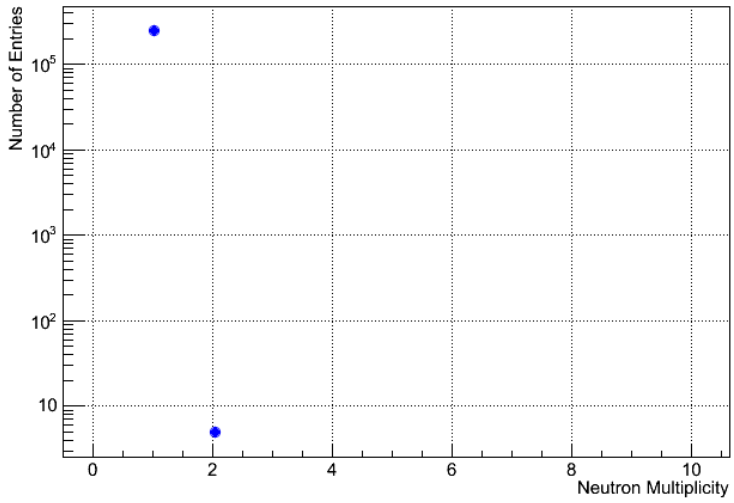

Fig. 35. Number of events containing a fast neutron vs neutron multiplicity recorded our liquid scintillator array during a period of 8 hrs. in the absence of a Pb pile.

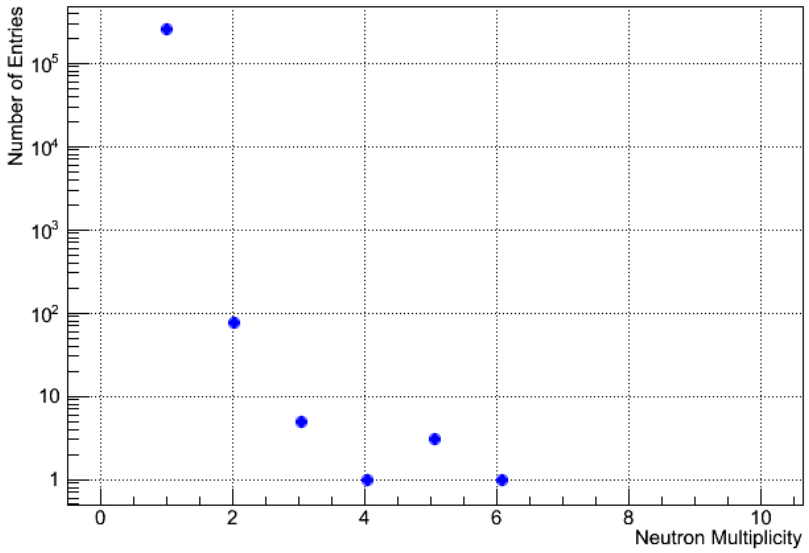

Fig. 36. Number of events containing a fast neutron vs neutron multiplicity recorded our liquid scintillator array during a period of 8 hrs. in the presence of Pb pile.

As is evident comparing Figures 35 and 36 the number of events with 4 or more fast neutrons increases dramatically in the presence of the Pb pile. In Fig. 37 we show a typical time history for bursts containing 5 or more neutron as measured in our detector array over a period of 8 hrs. As is evident from this time history our liquid scintillator array is seeing large bursts of fast neutron and γ-ray bursts with a very short time duration. The length of the lines in the upper picture indicates the number of particles in each burst. Since the effective efficiency of our liquid scintillator array is ~ 5%, these are events that contain 100 or more neutrons.

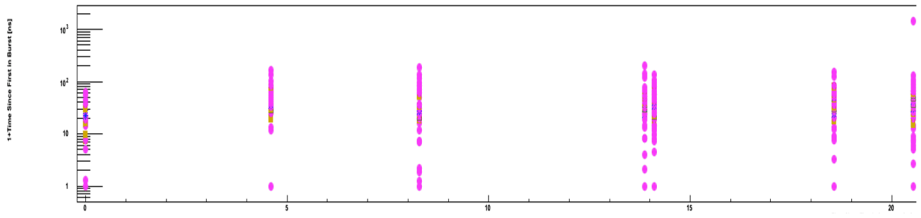

Fig. 37. Typical time history for fast neutron bursts containing at least 5 neutrons as recorded in our liquid scintillator array in the presence of a 50cmx50cmx50cm Pb pile during a period of 8 hours.

Typical particle compositions for these bursts are shown in Figures 38-39. As is evident from these figures the most common type of particle in a burst is a γ-ray. Figure 39 shows an example of a burst containing 9 observed neutrons. The fact that the MIP signals occur in the middle of these bursts suggests that these MIPs signals are not secondary cosmic ray muons, which we would expect to be recorded either

at the onset of the burst or at a far later time. Instead the MIPs signals appear to have been generated in the Pb in association with the neutrons and γ-rays.

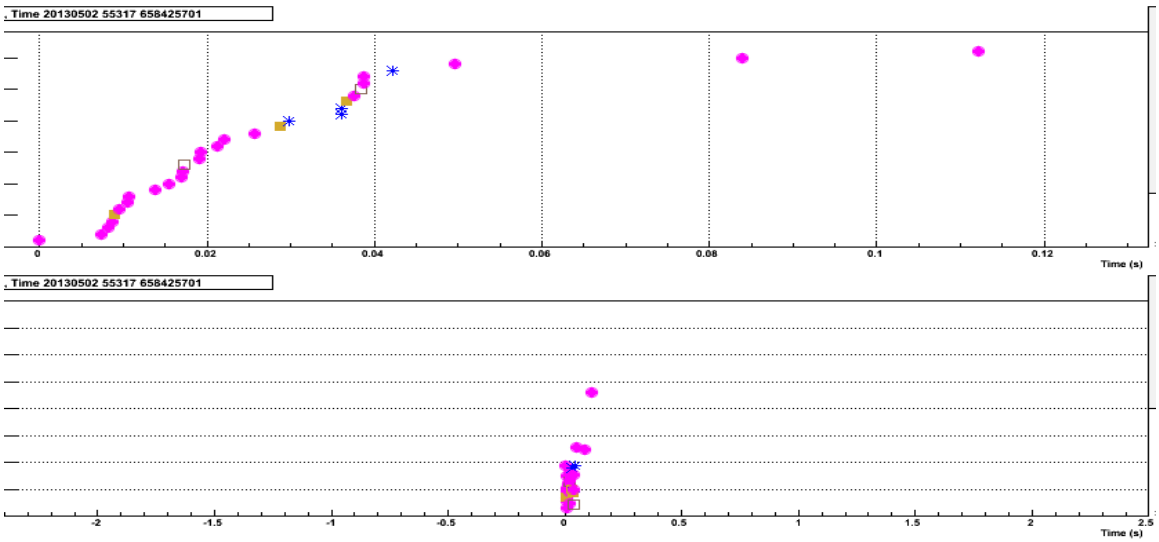

Fig. 38. Observed particle composition and time scale for a typical burst. The pink dots represent γ-rays, the blue dots represent MIPs, and the bronze squares represent fast neutrons. The time scale used in the upper graph is in units of shakes (10^{-8} sec).

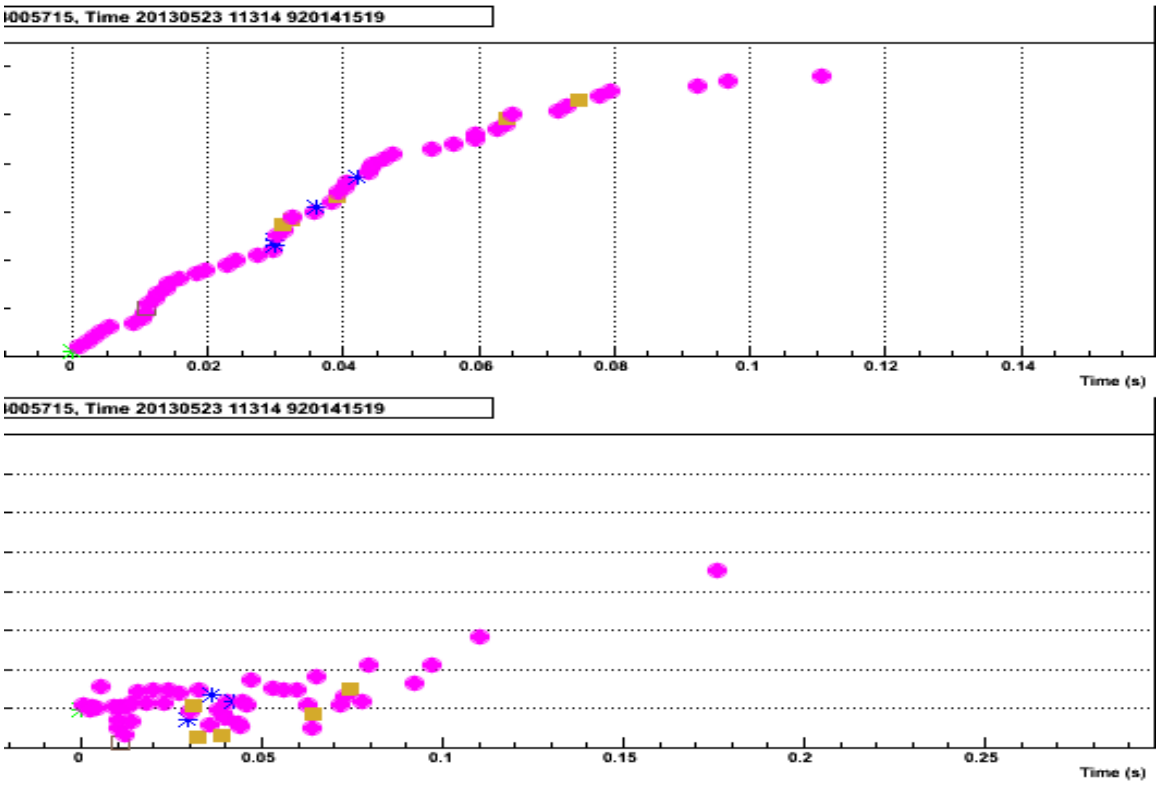

Fig. 39. Composition of a burst with 9 fast neutrons. The pink dots represent γ-rays, the blue dots represent MIPs, and the bronze squares represent fast neutrons. The upper graph shows the total counts, while the lower graph shows the time difference between successive particles in nanoseconds. The time scales for both graphs is in units of shakes (10^{-8} sec).

We have seen that seen that in the presence of a Pb pile bursts of fast neutrons are always accompanied by bursts of liquid scintillator γ-rays. Our main interest in this project though was to determine the origin of the MIP signals which seem to be correlated with the large neutron bursts from the Pb pile. In order to determine whether the MIP signals in the plastic scintillators that accompanied the neutron bursts were due to secondary cosmic ray muons or tertiary particles produced in the Pb pile, we investigated what would happen to the MIP signals when 4 of the plastic scintillator panels were moved to a distance of 11 feet from the Pb pile. The layout of our detector array with this configuration of plastic panels is illustrated in Figure 40.

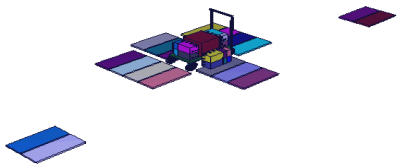

Fig. 40 Schematic diagram of detector array after 4 of the plastic scintillator panels were moved outward 11' from the Pb pile.

In Figure 41 we show the number of MIP signals recorded in the various plastic scintillators following a neutron signal recorded in 1 of the liquid scintillator cells. Overall the spatial distribution of MIP signals is in reasonable agreement with our Monte Carlo simulations (cf. Figure 28 which shows the count distribution before the 4 panels were moved). The difference in the number of MIP counts in the panels that were moved before and after being moved can be accounted for by just the $1/r^2$ decrease in the solid angle subtended by the panels. This is a strong hint that the MIP signals are mainly due to particles emitted from the Pb pile. This conclusion is strongly supported by looking at the distribution of neutron multiplicities for fast neutron bursts associated with a MIP signal.

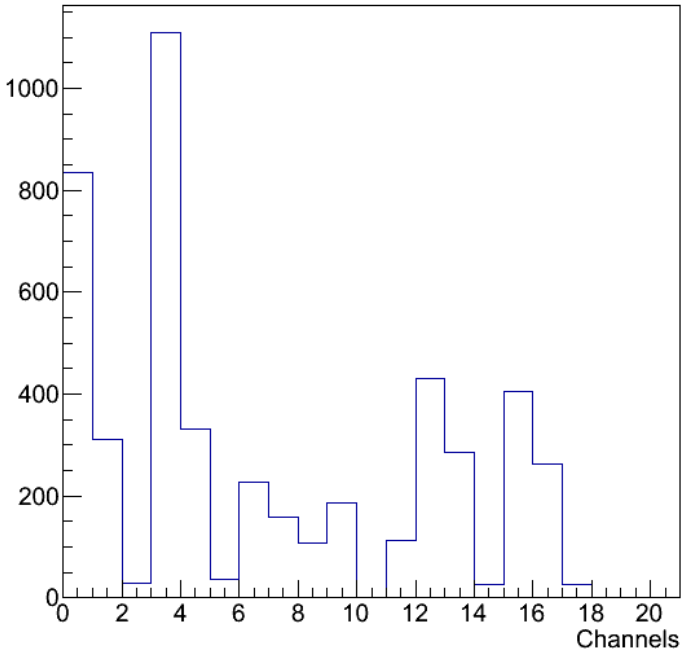

Fig. 41. Spatial distribution of MIP counts among the plastic scintillators (minus channel 11 which was not operational for this run) for MIP events initiated by a fast neutron signal in one of the liquid scintillators during an 8 hour period.

In Figure 42 we show the frequency vs size distribution for fast neutron bursts triggered by a MIP signal in one of the 4 plastic scintillators that were moved 11' from the Pb pile as illustrated in Figure 40, both before and after being moved. The rates of fast neutron bursts shown in these plots is close to what would be expected based on our Monte Carlo simulations of neutron bursts initiated by high energy secondary neutrons hitting the Pb pile (cf Figures 20 and 26). Moreover, the independence of these measured distributions on the position of the plastic scintillator is strong evidence that the MIP signals are directly associated with the neutron bursts.

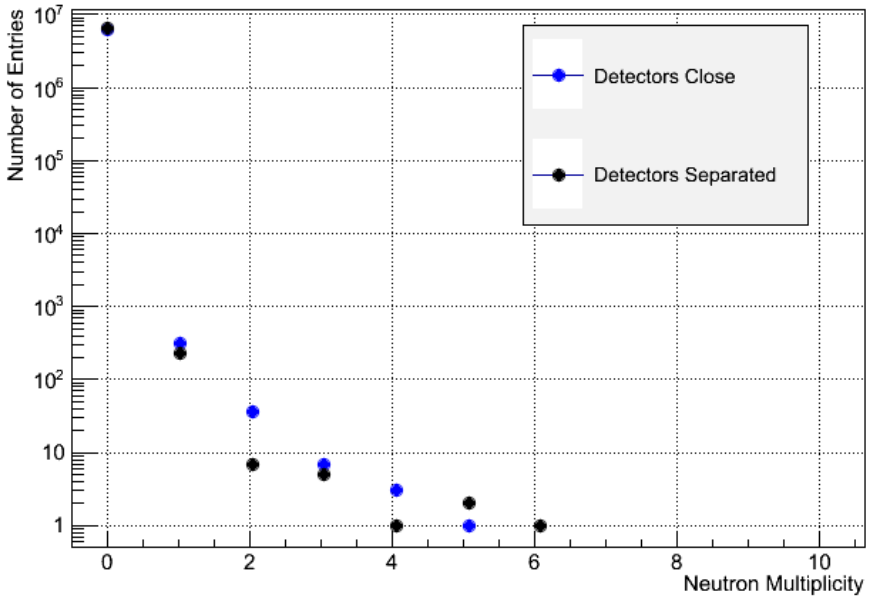

Fig. 41. Distribution of neutron burst sizes for bursts initiated by a MIP signal in one of 4 plastic scintillators for 16 hours of data.

It can be seen that the fast neutron burst multiplicity distribution for bursts accompanying a MIP is almost independent of the position of the plastic scintillators. This is strong evidence that the MIP signals are actually originating in the Pb pile in association with the neutron bursts. If we let A denote the recording of MIP signal and B_i denote the simultaneous recording of *i* fast neutrons, then it follows from Bayes Theorem that

$$p(B_i \mid A) = p(A \mid B_i)p(B_i) / p(A),$$

where the total probability of getting a MIP signal is:

$$p(A) = \sum_i p(A \mid B_i)$$

We now want to compare $p(B_i|A)$ for the two configurations of plastic scintillator panels shown in Figures 21 and 40. If all the MIP signatures recorded in the plastic

scintillators originated in the Pb pile then the probability $p(A_s|B_i)$ for obtaining a MIP signal detected in 1 of the 4 shifted panels shown in Figure 40 when there is a burst of i neutrons will be related to the probabilities $p(A_0|B_i)$ for the same 4 panels before they were shifted by

$$p(A_s \mid B_i) = \lambda p(A_0 \mid B_i),$$

where λ is geometric factor determined by the amount of shift. Since λ doesn't depend on the neutron multiplicity, it cancels out in the Bayes formula, leaving us with the result that the multiplicity distribution is independent of the distance of the of the plastic scintillator panels from the Pb pile:

$$p(B_i \mid A_s) = p(B_i \mid A_0).$$

In Figures 42-43 we show the number of minimum ionizing particles (MIPS) recorded in the plastic scintillator panels during a random 128 ns time window as a function of the number of liquid scintillator fast neutrons recorded in the same time window. The difference in the scale of the horizontal axes in Figures 42 and 43 should be noted, along with the fact that the presence of the Pb pile leads to MIP bursts associated with large fast neutron bursts.

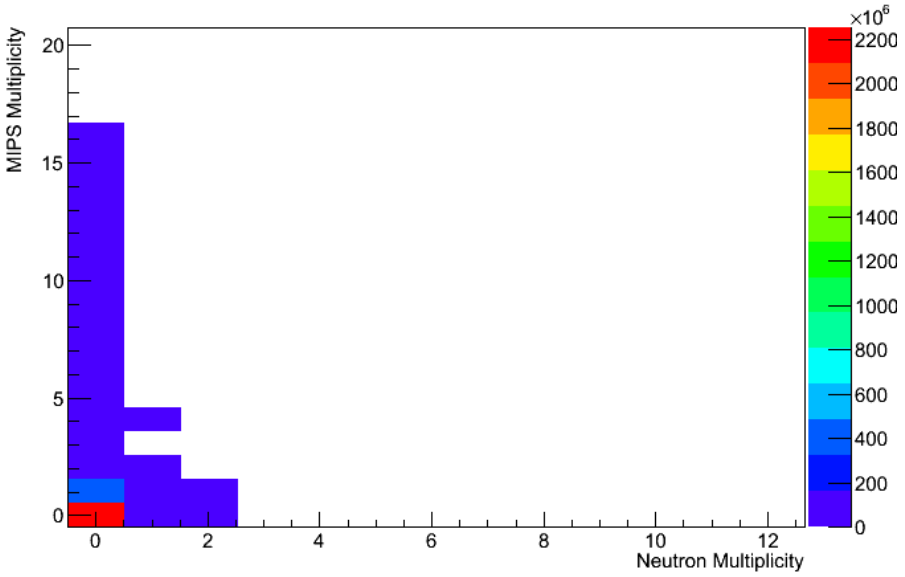

Fig. 42. Observed correlations between liquid scintillator neutron multiplicites and plastic scintillator MIP multiplicities in the absence of a 50cmx50cmx50cm Pb brick pile for 5.33 days of data.

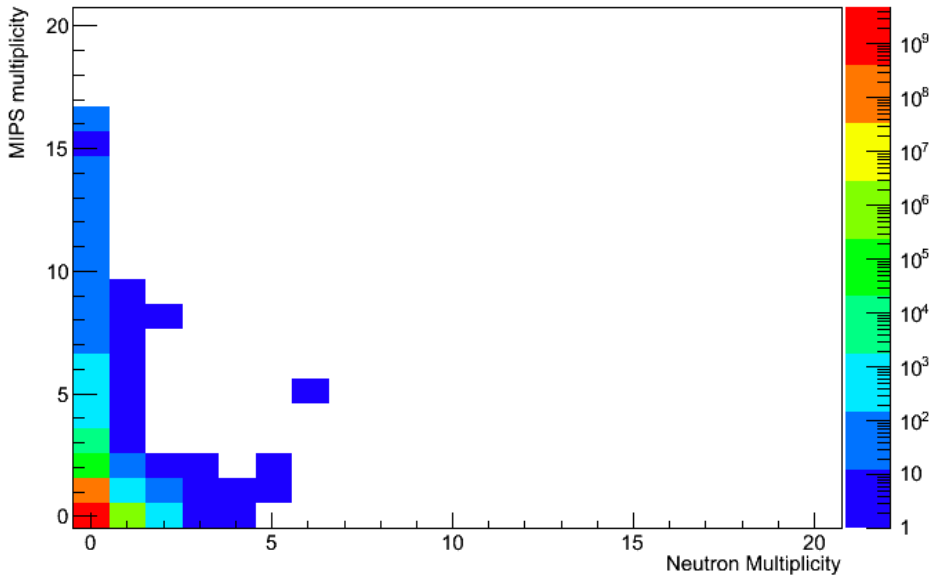

Fig. 43. Observed correlations between liquid scintillator neutron multiplicites and plastic scintillator MIP multiplicities in the presence of our 50cmx50cmx50cm Pb brick pile for 5.33 days of data.

Conclusions

Our 2006 Pb pile experiment showed that cosmic ray interactions with a Pb pile produce very large neutron bursts at a surprisingly high rate, and these large bursts were always accompanied by minimum ionizing particles that we interpreted as being muons. One of the principal findings of this project is that the MIP signals that we had previously interpreted as being due to cosmic ray muons are almost certainly due to tertiary minimum ionizing particles produced in the Pb pile by secondary cosmic rays, and not secondary cosmic ray muons. There are events where neutron bursts are produced in coincidence with secondary cosmic ray muons, but these events are relatively rare. Indeed our simulation results suggest that when a fast neutron signal is recorded in a liquid scintillator detector next to the Pb pile, then there is only a very small probability $\sim 10^{-7}$ that a secondary cosmic ray muon will be detected simultaneously in a plastic scintillator located anywhere in the vicinity of the pile.

Apart from accidental coincidences between secondary cosmic ray muons and secondary cosmic ray neutrons, the two main effects that contribute to correlations between cosmic ray produced neutrons and muons are 1) neutrons produced by the capture of secondary cosmic ray muons in the soil or detectors, and 2) production of tertiary neutrons and pions produced by interactions of high energy secondary neutrons with materials not far from the neutron detector. Of these two processes the first is the most important under ordinary circumstances. In particular, both our

Monte Carlo simulations and experiment have suggested that the average coincidence rate between secondary cosmic ray muons signals detected in a plastic scintillator and muon capture neutrons detected in a liquid scintillator array located nearby will be approximately 5/minute. On the other hand, in the case of tertiary muons resulting from pion decay, the muons can only be detected only at distances > pion decay length which is ~ 10m. This means that the probability of detecting a coincident tertiary muon and neutron is diluted by a large geometric factor. Assuming that one used 1 m^2 plastic and liquid scintillator arrays to detect a coincident tertiary neutron and muon the count rate would be less than 1 per year. Of course, in the presence of a ton of high Z material such as Pb there will be very large bursts of neutrons accompanied by comparable numbers of MIPs; however, our observations and simulations imply that the rate of these events is only about 1 per hour. Although the detection rate for coincident tertiary neutrons and muons in this case could be substantially increased by placing the neutron detector next to the high Z material, simultaneous observation of the tertiary neutrons and muons from these events does not appear to be a useful method for searching for nuclear materials.

One very positive result of our investigations is that we have found a plausible explanation for the origin of the large neutron bursts observed in our 2006 Pb pile experiment and also noted in the 2008 "ship effect" paper of Kouzes et. al.: namely, we have found that primary cosmic protons interacting at an altitude a few km above sea level provide a good description for the phenomenology of low multiplicity bursts while a 1 TeV proton incident on the top of the atmosphere provides a good description of the phenomenology of the largest bursts that were observed. Understanding these effects is crucial for obtaining a detailed understanding of the cosmic ray background; which in turn is crucial for the problem of stand-off detection of nuclear materials.

Another bright hope though is that significant production of pions associated with large neutron bursts from a Pb pile may provide a handy method for identifying high Z materials located not far from the Pb pile. For example, one might look for the characteristic neutron and γ-ray signatures from the pions and pion-decay muons that stop in high Z materials near to the Pb pile. In particular, looking for the time correlations between fast neutrons detected near to the Pb pile, and γ-rays detected with a detector with fast timing and good spectral resolution placed not far from the object of interest might provide a practical method for identifying high Z materials that have been selected for further examination using, e.g. x-ray radiography or muon tomography.

Acknowledgements

This work was performed under the auspices of the U.S. Department of Energy by Lawrence Livermore National Laboratory under Contract DE-AC52-07NA27344.